Cortical fosGFP expression reveals broad receptive field excitatory neurons targeted by POm

Jouhanneau, J.S., Ferrarese, L., Estebanez, L., Audette, N.J., Brecht, M., Barth, AL., Poulet, J.F.A.

Neuron
2014 DEC 03 ; 84(5): 1065-1078
doi: 10.1016/j.neuron.2014.10.014
Publisher: Cell Press / Elsevier

Cortical cfos Expression Reveals Broad Receptive Field Excitatory Neurons Targeted by POm

Jean-Sébastien Jouhanneau[1,2], Leiron Ferrarese[1,2], Luc Estebanez[1,2], Nick Audette[3], Michael Brecht[2,4], Alison L. Barth[3] and James F.A. Poulet[1,2]

[1]Department of Neuroscience, Max Delbrück Center for Molecular Medicine (MDC), Berlin-Buch, Robert-Rössle-Str. 10, 13092 Berlin, Germany.
[2]Cluster of Excellence NeuroCure, Neuroscience Research Center, Charité-Universitätsmedizin Berlin, Charitéplatz 1, 10117 Berlin, Germany.
[3]Department of Biological Sciences and Center for the Neural Basis of Cognition, Carnegie Mellon University, 4400 Fifth Avenue, Pittsburgh, PA 15213, USA.
[4]Bernstein Center for Computational Neuroscience (BCCN), Humboldt University Berlin, Philippstrasse 13, 10115 Berlin, Germany.

Correspondence to be addressed to:

James Poulet,
Department of Neuroscience,
Max-Delbrück-Center for Molecular Medicine (MDC),
Robert-Rössle-Str. 10,
10392 Berlin-Buch,
Germany.

Telephone: +49 (0)30 450 639795
Fax: +49 (0)30 450 539979
E-Mail: james.poulet@mdc-berlin.de
Website: http://www.mdc-berlin.de/poulet

Total file length, 72249 characters

RUNNING TITLE

Broad receptive field pyramidal neurons

SUMMARY

Neighboring cortical excitatory neurons show considerable heterogeneity in their responses to sensory stimulation. We hypothesized that a subset of layer 2 excitatory neurons in the juvenile (P18 to 27) mouse whisker somatosensory cortex, distinguished by expression of the activity-dependent fosGFP reporter gene, would be preferentially activated by whisker stimulation. In fact, two-photon targeted, dual whole-cell recordings showed that principal whisker stimulation elicits similar amplitude synaptic responses in fosGFP-expressing and fosGFP^{-} neurons. FosGFP^{+} neurons instead displayed shorter latency and larger amplitude subthreshold responses to surround whisker stimulation. Using optogenetic stimulation we determined that these neurons are targeted by axons from the posteromedial nucleus (POm), a paralemniscal thalamic nucleus associated with broad receptive fields and widespread cortical projections. We conclude that fosGFP expression discriminates between single- and multi-whisker receptive field layer 2 pyramidal neurons.

INTRODUCTION

A common feature of sensory processing in cortex is the response heterogeneity of neighboring neurons, especially in superficial layers (Barth and Poulet, 2012). The source of this heterogeneity has been the subject of much speculation. Differences in sensory-evoked responses may arise from moment-to-moment variations in ongoing activity, stochastic processes (such as synaptic plasticity) that generate feature-specific ensembles, or specified wiring. Recently, sensory response properties and wiring differences have been investigated in cortical GABA-ergic interneuron subtypes (Adesnik et al., 2012; Gentet et al., 2012; Hofer et al., 2011; Kerlin et al., 2010; Kuhlman et al., 2011; Runyan et al., 2010). In contrast, the neural mechanisms underlying sensory response heterogeneity in excitatory neurons are unknown.

Does response heterogeneity in pyramidal neurons result from differences in how they are wired into the neocortical circuit? Current evidence is mixed. Broad receptive field subthreshold responses, observed in visual and somatosensory cortex (Brecht et al., 2003; Carandini and Ferster, 2000; Haider and McCormick, 2009; Higley and Contreras, 2003; Moore and Nelson, 1998; Runyan et al., 2010; Varga et al., 2011; Zhu and Connors, 1999), indicate an all-to-all connectivity scheme. Alternatively, feature-specific ensembles of neurons linked by synaptic connections have been observed in visual cortex (Ko et al., 2011), and brain slice studies suggest nonrandom, selective connectivity among neocortical excitatory neurons within and across layers (Anderson et al., 2010; Brown and Hestrin, 2009; Perin et al., 2011; Song et al., 2005; Yoshimura et al., 2005).

Separate from intracortical connectivity, subcortical input might be differentially distributed across excitatory neurons. This is certainly the case between neocortical layers in the somatosensory whisker system, where the thalamic posteromedial nucleus (POm) preferentially terminates in L5A and L1, and ventral posteromedial nucleus (VPM) afferents terminate in L5B and L4 (Koralek et al., 1988; Lu and Lin, 1993; Ohno et al., 2012; Pierret et al., 2000; Wimmer et al., 2010). Evidence for the continued segregation of these pathways within the cortex is debated (Bureau et al., 2006; Feldmeyer, 2012; Kim and Ebner, 1999). Overall, it remains unknown whether response heterogeneity in neighboring excitatory neurons is related to differences in the

distribution of subcortical or intracortical inputs. Resolution of this issue will have important implications for how neocortical circuits develop and can be modified by experience.

Here we used in vivo visually targeted dual whole-cell recordings to compare the sensory-evoked responses of neighboring excitatory, pyramidal neurons in superficial layer 2 of somatosensory cortex. In vivo whole-cell recordings allow analysis of the earliest thalamically evoked synaptic input, providing a more direct link to sensory input wiring differences than later evoked spiking, which will be subject to intracortical processing. Furthermore, simultaneous recordings allow a direct comparison of the subthreshold response of different neurons to the same sensory stimulus, removing experimental variability inherent to sequential in vivo recordings. Because there are no molecular markers for excitatory cell subsets in superficial layers of the cortex, we used expression of the activity-dependent reporter fosGFP to distinguish between pyramidal neurons (Barth et al., 2004; Yassin et al., 2010).

We predicted that fosGFP-expressing neurons ($fosGFP^+$) would show stronger sub- and supra-threshold responses to sensory stimulation than unlabeled ($fosGFP^-$) neurons. This would be consistent with in vitro studies indicating that $fosGFP^+$ neurons show a larger excitatory response to extracellular layer 4 stimulation than $fosGFP^-$ neurons (Benedetti et al., 2013). In fact, we show that stimulation of the center of the receptive field triggered similar amplitude subthreshold responses in $fosGFP^-$ and $fosGFP^+$ neurons. Stimulation of the surrounding receptive field, however, elicited a consistent shorter latency and larger amplitude subthreshold response in $fosGFP^+$ neurons. Channelrhodopsin-2 (ChR2)-mediated stimulation of the POm of the thalamus, a nucleus associated with broad receptive field responses, revealed faster and larger amplitude subthreshold input to $fosGFP^+$ neurons compared to neighboring $fosGFP^-$ neurons.

Our data suggest that broad receptive field input is a critical parameter of feature encoding in the barrel cortex that can drive fosGFP expression in layer 2 pyramidal neurons. $FosGFP^+$ neurons may therefore overlap with broad receptive field neurons identified in previous studies (Estebanez et al., 2012; Ghazanfar and Nicolelis, 1997; Sato and Svoboda, 2010). Moreover,

our data indicate that broad receptive field neurons in layer 2 are targeted by POm.

RESULTS

Dual Two Photon Targeted Whole-Cell Recordings Confirm Higher Spontaneous Firing Rates in fosGFP+ Neurons

In the fosGFP mouse, approximately 10% to 20% of layer 2 excitatory neurons in somatosensory (barrel) cortex exhibit nuclear labeling for fosGFP and can be visualized and targeted using in vivo two photon imaging (Barth et al., 2004; Yassin et al., 2010) (Figure S1 available online). To compare sensory response properties across layer 2 neurons differentiated by activity-dependent gene expression, we used dual whole-cell recordings targeted to neighboring fosGFP$^+$ and fosGFP$^-$ neurons in urethane-anesthetized P18 to P27 mice (mean depth –159.1 ± 4.6 μm below the pial surface; mean soma distance 50.7 ± 3.7 μm, n = 52 pairs). A <1 mm diameter craniotomy was drilled over the barrel cortex and two to three whole-cell pipettes filled with intracellular solution and Alexa 594 were inserted into layer 2. FosGFP$^+$ neurons were visible using 930 nm light, while neighboring unlabeled cells appeared as dark shadows against a background of red Alexa-594-stained extracellular space using 820 nm light (Kitamura et al., 2008). Excitatory neurons were identified by their evoked regular-spiking phenotype, in vivo fluorescent images (including the presence of dendritic spines), and post hoc biocytin staining (Figures S2 and S3). FosGFP$^+$ neurons have a slightly, but significantly, larger soma size than fosGFP$^-$ neurons (fosGFP$^+$ 209.9 ± 24.8 μm^2 versus fosGFP$^-$ 189.5 ± 22.5 μm^2, n = 18 pairs, p = 0.003), but we did not identify a distinct dendritic branching pattern or axonal target structure (Figures S3 and S4).

Previously we have reported that fosGFP$^+$ neurons exhibit higher spontaneous firing rates in vivo, using juxtacellular recordings (Yassin et al., 2010). Dual whole-cell recordings of layer 2 neurons confirm this and show that spontaneous firing was two times higher in fosGFP$^+$ compared to fosGFP$^-$ neurons (fosGFP$^+$ 0.18 ± 0.06 Hz versus fosGFP$^-$ 0.09 ± 0.04 Hz, n = 7 pairs, p = 0.031) (Figures S2D and S2G). Under urethane anesthesia,

cortical neurons oscillate between periods of quiescent, hyperpolarized Downstates and active, depolarized Upstates. Downstate membrane potential (V_m) was similar, as was spike threshold (V_{rest} fosGFP$^+$ –62.89 ± 1.94 mV versus fosGFP$^-$ –60.59 ± 2.30 mV, n = 7 pairs, p = 0.375; V_{thresh} fosGFP$^+$ –36.98 ± 1.65 mV versus fosGFP$^-$ –35.10 ± 1.22 mV, n = 7 pairs, p = 0.109). There were small but significant differences, however, in the kinetics of the Upstate, with fosGFP$^+$ neurons showing a faster onset and larger charge transfer during the Upstate (onset slope fosGFP$^+$ 76.53 ± 7.48 mV/ms versus fosGFP$^-$ 56.95 ± 7.69 mV/ms, n = 7 pairs, p = 0.016; charge transfer fosGFP$^+$ 14.92 ± 1.80 mV·ms versus fosGFP$^-$ 12.96 ± 1.56 mV·ms, n = 7, p = 0.016).

Principal Whisker Stimulation Evokes Similar Subthreshold Responses in fosGFP$^+$ and fosGFP$^-$ Neurons

Dual whole-cell recordings allowed us to compare not only the firing rates of layer 2 neurons but also the subthreshold synaptic input that drives spiking. The short latency sensory-evoked synaptic response reflects both direct thalamic and recurrent cortical inputs into the layer 2 network. To isolate this response for comparison between cells, we focused analysis on the earliest synaptic response: the first 30 ms following whisker deflection. Responses were averaged over multiple trials (8 to 57 trials per cell), and then compared across all pairs within the respective dataset.

Initially we hypothesized that fosGFP$^+$ neurons might simply receive more overall sensory input and that this input might be sufficient to explain the activity-dependent gene expression in these neurons. Consistent with this, acute brain slice recordings indicate that fosGFP$^+$ neurons receive stronger excitatory drive from layer 4 electrical stimulation compared to adjacent fosGFP$^-$ neurons in layers 2 and 3 of barrel cortex (Benedetti et al., 2013).

The anatomy of the barrel field allows recordings to be made from identified, specific whisker-responsive cortical columns. Dual whole-cell recordings were targeted to the C2 barrel column using intrinsic optical imaging (Figures 1A and 1B). Piezo-driven C2 whisker deflection reliably evoked short latency subthreshold responses (Figures 1C and 1F). We saw no significant difference in sensory response latency during stimulation of the principal whisker (Figures 1D to 1I; fosGFP$^+$ 11.86 ± 0.72 ms versus fosGFP$^-$

12.33 ± 0.52 ms; n = 17 pairs, p = 0.353). There was also no difference in response amplitude (Figure 1J; fosGFP$^+$ 5.09 ± 0.60 mV versus fosGFP$^-$ 5.77 ± 1.07 mV; n = 17 pairs, p = 0.818), or the response onset slope (Figure 1K, fosGFP$^+$ 0.49 ± 0.10 mV/ms versus fosGFP$^-$ 0.63 ± 0.18 mV/ms; n = 17 pairs, p = 0.782). Piezo stimulation was insufficient to generate short latency spikes in the majority of cells examined; accordingly we observed no significant difference in piezo-evoked firing between cells. These data indicate that principal whisker synaptic inputs, most likely mediated by VPM thalamic drive, are similar between fosGFP$^+$ and fosGFP$^-$ neurons.

FosGFP$^+$ Neurons Show Larger and Earlier Responses to Multiple Whisker Stimulation.

Mice and rats monitor their nearby tactile environment with an array of whiskers that simultaneously contact objects and surfaces (Carvell and Simons, 1990). Next, we therefore investigated the response of fosGFP$^+$ and fosGFP$^-$ neurons to airpuff-evoked multiple whisker stimulation using two-photon targeted dual whole-cell recordings in untargeted barrel columns (Figures 2A and 2B).

Analysis of the initial synaptic sensory response unexpectedly showed a markedly shorter depolarizing onset latency for fosGFP$^+$ neurons across individual trials (Figures 2C and 2D) and also in averaged traces (Figures 2E, 2F, and 2I; fosGFP$^+$ 9.74 ± 0.52 ms versus fosGFP$^-$ 12.52 ± 1.58 ms; n = 10 pairs, p = 0.049), with a difference of 2.8 ms. These results suggest that the sensory-evoked response latency is a fixed property of a cell within the network, rather than a stochastic property regulated by moment-to-moment changes in the cortical network.

FosGFP$^+$ neurons also showed a larger subthreshold response amplitude in the first 30 ms after stimulus onset (Figures 2G and 2I; fosGFP$^+$ 3.24 ± 1.11 mV versus fosGFP$^-$ 1.99 ± 0.81 mV, n = 10 pairs, p = 0.027). The rise of the early response slope was also significantly steeper in fosGFP$^+$ neurons (Figure 2H and 2I, fosGFP$^+$ 0.44 ± 0.17 mV/ms versus fosGFP$^-$ 0.26 ± 0.1 mV/ms; n = 10 pairs, p = 0.049). In contrast to single, principal whisker stimulation (Figure 1), these data indicate that fosGFP$^+$ neurons receive

greater synaptic drive during multiple whisker stimulation as compared to fosGFP$^-$ neurons.

We next compared firing rates between fosGFP$^+$ and fosGFP$^-$ during airpuff stimulation of the contralateral whisker pad (Figure 3). We observed low overall rates of airpuff-induced firing, and only a few spikes were ever observed at short latency (<50 ms). However, whisker airpuff induced a prolonged depolarization in all cells, with low numbers of spikes distributed over the 1.5 s following the stimulus (Figure 3A and 3B). FosGFP$^+$ neurons exhibited significantly more airpuff-associated spikes (Figure 3C and 3D) (fosGFP$^+$ 1.02 ± 0.56 versus fosGFP$^-$ 0.63 ± 0.38 spikes/stim; n = 10 pairs, p = 0.039). We also noticed that the synaptic charge measured during the prolonged response was significantly larger in fosGFP$^+$ than fosGFP$^-$ neurons (Figure 3E; fosGFP$^+$ 13.67 ± 1.57 versus fosGFP$^-$ 11.68 ± 1.37 mV·s; n = 10 pairs, p = 0.014). Untargeted multi-whisker airpuff stimulation therefore induces larger synaptic drive and more spikes in fosGFP$^+$ neurons.

Multiwhisker Stimulation Directed to the Principal Whisker Row Triggers Similar Synaptic Responses in fosGFP$^+$ and fosGFP$^-$ Neurons

What is the source of the afferent drive that triggers an earlier and larger response in fosGFP$^+$ neurons? Previous studies in barrel cortex have shown that some layer 2 excitatory neurons have broad subthreshold receptive fields, receiving synaptic input during stimulation from the principal whisker as well as surrounding whiskers (Brecht et al., 2003; Moore and Nelson, 1998; Varga et al., 2011; Zhu and Connors, 1999). Because multi-whisker airpuff stimulation preferentially targets fosGFP$^+$ neurons (Figure 2), we hypothesized that the short-latency, high-amplitude responses in fosGFP$^+$ neurons might arise from the stimulation of surrounding whiskers.

To compare the responses of fosGFP$^+$ and fosGFP$^-$ neurons to stimulation of principal and surrounding whiskers, we first targeted dual whole-cell recordings to a C row barrel and directed the airpuff stimulus toward the C row (Figures 4A and 4B). Similar to single, principal whisker stimulation, stimulation of the central row of whiskers by an airpuff elicited similar synaptic responses in fosGFP$^+$ and fosGFP$^-$ neurons (Figures 4C-4E). Across the population, the latency (Figures 4F; fosGFP$^+$ 7.48 ± 0.66 ms

versus fosGFP$^-$ 7.80 ± 0.44 ms; n = 7 pairs, p = 0.469), amplitude (Figure 4G; fosGFP$^+$ 7.47 ± 2.44 mV versus fosGFP$^-$ 8.12 ± 2.69 mV; n = 7 pairs, p = 0.813) and onset slope (Figure 4H; fosGFP$^+$ 1.06 ± 0.41 mV/ms versus fosGFP$^-$ 1.44 ± 0.60 mV/ms; n = 7 pairs, p = 0.297) showed no significant difference. Thus, deflection of the principal whisker, whether as a single whisker (Figure 1) or together with surrounding whiskers (Figure 4), evokes no difference in the early synaptic response between fosGFP$^+$ and fosGFP$^-$ neurons. These data suggest that principal whisker stimulation is unlikely to drive immediate early gene expression.

Stimulation of Surround Whiskers Differentiates Synaptic Response Properties

To compare the responses of fosGFP$^+$ and fosGFP$^-$ neurons to deflection of surrounding whiskers, we next targeted recordings to the A row and directed the airpuff stimulus toward the E row, the most distant row of whiskers on the mystacial pad (Figures 5A and 5B). Stimulation of the distant E row whiskers elicited significantly shorter latency responses in fosGFP$^+$ in comparison to fosGFP$^-$ cells (Figures 5C-5F; fosGFP$^+$ 13.45 ± 1.04 ms versus fosGFP$^-$ 18.47 ± 1.82 ms, n = 8 pairs, p = 0.008). The latency of the fosGFP$^-$ neuron response trailed the subthreshold response in fosGFP$^+$ neurons by 5 ms, a greater difference than observed in experiments where recordings were not directed to a specific location in the barrel field (Figure 2).

Furthermore, the mean response amplitude (Figure 5G; 1.07 ± 0.26 mV in fosGFP$^+$ neurons versus 0.43 ± 0.16 mV in fosGFP$^-$; n = 8, p = 0.023) and the onset slope (Figure 5H, fosGFP$^+$ 0.16 ± 0.03 mV/ms versus fosGFP$^-$ 0.07 ± 0.02 mV/ms; n = 8 pairs, p = 0.016) of the synaptic response were larger in fosGFP$^+$ compared to fosGFP$^-$ neurons. These data are therefore consistent with the hypothesis that fosGFP$^+$ neurons receive stronger synaptic drive from stimulation of surround whiskers.

Single-Whisker Stimulation to Evaluate Surround Whisker Synaptic Input

Airpuff stimulation deflects multiple whiskers. To have better control of individual whisker movements and to examine the receptive field in more

detail, we next performed dual whole-cell recordings in the C2 barrel column and interleaved deflection of the principal whisker (C2) and a surround whisker (B2) with a piezo-driven glass rod (Figures 6A-6H) (n = 10 interleaved pairs). B2 whisker stimulation elicited shorter latency (Figure 6I; fosGFP$^+$ 12.95 ± 0.82 ms versus fosGFP$^-$ 17.17 ± 1.74 ms; n = 10 pairs, p = 0.002), larger amplitude responses (Figure 6J; fosGFP$^+$ 4.03 ± 0.76 mV versus fosGFP$^-$ 1.96 ± 0.29 mV; n = 10 pairs, p = 0.002) with faster onset slopes (Figure 6K; fosGFP$^+$ 0.37 ± 0.08 mV/ms versus fosGFP$^-$ 0.12 ± 0.02 mV/ms; n = 10 pairs, p = 0.002) in fosGFP$^+$ as compared to fosGFP$^-$ cells. Therefore, we conclude that fosGFP$^+$ neurons have a broader receptive field than fosGFP$^-$ neurons whether stimulating multiple or single whiskers.

Thalamic Optogenetic Stimulation Reveals Stronger POm Input to fosGFP$^+$ Neurons

The broad receptive fields of fosGFP$^+$ neurons might arise from direct thalamic input and/or through recurrent connections within the cortical column (Bureau et al., 2006; Fox et al., 2003). Somatosensory whisker thalamus is composed of two major cortically projecting nuclei, POm and VPM. VPM thalamic neurons show predominantly short latency, single-whisker receptive fields. POm thalamic neurons exhibit characteristically large receptive fields, showing nearly equivalent responses to stimulation of different whiskers (Ahissar et al., 2000; Chiaia et al., 1991; Diamond et al., 1992), and can show short latency spiking responses with low frequency multi-whisker stimulation (Figure S5) (Ahissar et al., 2000; Diamond et al., 1992; Masri et al., 2008; Sosnik et al., 2001).

We first tested whether VPM input could target fosGFP$^+$ neurons. VPM was targeted for virus-mediated expression of ChR2 (Boyden et al., 2005). Two weeks later, in order to allow time for ChR2 protein expression, an optical fiber was positioned in VPM and a brief (3 ms) pulse of blue light was delivered to activate virally transduced neurons during dual whole-cell recordings of layer 2 fosGFP$^+$ and fosGFP$^-$ neurons (Figures 7A and 7B). The infection locus was verified by post-hoc histology, indicating a center of infection located in the VPM, and was supported by the characteristic distribution of VPM axons in layer 4 and 5B (Koralek et al., 1988; Lu and Lin,

1993; Ohno et al., 2012; Wimmer et al., 2010) (Figures 7B and S6F). Optogenetic stimulation of VPM triggered reliable short latency inputs to all layer 2 pyramidal neurons we recorded (Figures 7C-7E). The early synaptic responses, however, did not show a significant difference in response latency (Figure 7F; fosGFP$^+$ 7.77 ± 1.52 ms versus fosGFP$^-$ 7.13 ± 0.81 ms; n = 6 pairs, p = 0.563), amplitude (Figure 7G; fosGFP$^+$ 5.38 ± 2.40 mV versus fosGFP$^-$ 4.98 ± 2.24 mV; n = 6 pairs, p = 0.563), or onset slope (Figure 7H; fosGFP$^+$ 0.82 ± 0.38 mV/ms versus fosGFP$^-$ 0.69 ± 0.28 mV/ms; n = 6 pairs, p=1) between fosGFP$^+$ and fosGFP$^-$ neurons.

We next tested whether POm input could differentiate between layer 2 neurons in fosGFP transgenic mice. POm was targeted for virus-mediated expression of ChR2, and dual whole-cell recordings were made during thalamic stimulation (Figure 8A and 8B). The infection locus was verified by post hoc histology, indicating a center of infection located in the POm, and was supported by the characteristic distribution of POm axons in layer 5A and layer 1 (Koralek et al., 1988; Lu and Lin, 1993; Ohno et al., 2012; Wimmer et al., 2010) (Figures 8B and S6C).

Optogenetic stimulation of POm neurons triggered a short latency subthreshold response in layer 2 neurons (Figures 8C-8E and 8I). ChR2-mediated POm activation revealed a statistically significant difference in the latency of the subthreshold response, where fosGFP$^+$ neurons consistently exhibited a 2.5 ms earlier response (Figure 8F; fosGFP$^+$ 6.50 ± 0.62 ms versus fosGFP$^-$ 8.96 ± 0.61 ms; n = 8 pairs, p = 0.008). The amplitude of the ChR2-mediated response was also significantly larger in fosGFP$^+$ neurons (Figure 8G; fosGFP$^+$ 2.62 ± 0.85 mV versus fosGFP- 1.73 ± 0.47 mV; n = 8 pairs, p = 0.039). Consistent with previous surround whisker stimulation data, the slope of the initial response was also significantly steeper, suggesting that these neurons are innervated by a larger number of POm-driven inputs (Figure 8H; fosGFP$^+$ 0.27 ± 0.14 mV/ms vs. fosGFP$^-$ 0.13 ± 0.05 mV/ms; n = 8, p = 0.039). Overall, the data show that L2 fosGFP$^+$ neurons receive more synaptic drive from POm activation than neighboring fosGFP$^-$ neurons.

DISCUSSION

Here we used dual two-photon targeted whole-cell recordings to compare sensory-driven synaptic input to layer 2 excitatory neurons differentiated by spontaneous activity and expression of the immediate-early gene, c-fos. Whole-cell recordings enable analysis not only of evoked firing, but also of subthreshold response properties, including response latency, that are robust indicators for how a neuron can be wired into a complex circuit. In contrast to sequential single recordings, dual recordings remove variability due to changes in brain state or sensory stimulus control across trials or animals seen in sequential single recordings and allow direct comparison of sensory input or ongoing activity (Crochet et al., 2011; Lampl et al., 1999; Okun and Lampl, 2008; Poulet and Petersen, 2008; Yu and Ferster, 2010). In addition, two-photon microscopy allows recordings to be targeted to genetically identified and anatomically neighboring neurons.

Using this approach, we identified a reliable and significant difference in response latency and amplitude that enabled us to differentiate the receptive field properties of fosGFP$^+$ neurons compared to neighboring, unlabeled cells. Stimulation of the center of the receptive field either by deflection of the single principal whisker, or by multi-whisker airpuff stimulation, provided similar synaptic drive to fosGFP$^+$ and fosGFP$^-$ neurons. In contrast, stimulation of the surround receptive field triggered earlier and larger synaptic response in fosGFP$^+$ neurons. In vivo optogenetic stimulation of POm, a somatosensory, “paralemniscal” thalamic nucleus characterized by multi-whisker responses (Ahissar et al., 2000; Chiaia et al., 1991; Diamond et al., 1992; Masri et al., 2008; Sosnik et al., 2001) and axons that spread over a wide cortical area (Ohno et al., 2012; Wimmer et al., 2010) similarly revealed a faster and larger subthreshold response in fosGFP$^+$ neurons compared to simultaneously recorded fosGFP$^-$ neurons. Our finding that fosGFP$^+$ neurons receive shorter latency input following surround whisker stimulation reveals an unexpected specificity in the receptive field of the afferent drive to layer 2 neurons.

Single- and Multi-Whisker Brainstem-to-Cortex Circuits

A common feature of sensory processing in cortical neurons across different modalities is the integration of broad-field subthreshold synaptic input to

generate sharply tuned action potential outputs (Carandini and Ferster, 2000; Haider and McCormick, 2009). Does broad receptive field input result from an all-to-all cortical connectivity scheme, or is there identifiable substructure in the thalamo-cortical wiring of broad receptive field cortical neurons? In the barrel cortex, layer 2/3 excitatory neurons respond with depolarizing synaptic input to stimulation of both the central principal whisker and also the surrounding whiskers (Brecht et al., 2003; Higley and Contreras, 2003; Moore and Nelson, 1998; Varga et al., 2011; Zhu and Connors, 1999), indicating a broad, nonspecific connectivity. However, specialized single- or multi-whisker neurons have been identified using extracellular recordings with high-resolution multiple whisker stimulation (Estebanez et al., 2012; Ghazanfar and Nicolelis, 1997; Sato and Svoboda, 2010). It is unclear how these different response properties are generated.

Single- and multi-whisker responsive neurons are present not only in cortical circuits but also at earlier stages of sensory processing within the thalamus and brainstem trigeminal nuclei. Neurons in the principal trigeminal nucleus (Pr5) are typically single-whisker responsive and project mainly to VPM (Rhoades et al., 1987; Veinante and Deschênes, 1999; Williams et al., 1994), while multi-whisker responsive Pr5 cells form a sparse projection to POm (Veinante et al., 2000). Neurons within the interpolaris division of the spinal trigeminal complex (Sp5i) typically respond to multiple whiskers and project to POm, but also show a sparse projection to VPM (Veinante et al., 2000). While VPM neurons can respond to multiple whiskers (Nicolelis et al., 1993; Simons and Carvell, 1989), they are dominated by a single-whisker input (Brecht and Sakmann, 2002; Friedberg et al., 1999; Waite, 1973) and project to single cortical barrel columns (Oberlaender et al., 2012; Pierret et al., 2000). POm neurons respond equally well to the stimulation of multiple individual whiskers (Diamond et al., 1992; Masri et al., 2008; Sosnik et al., 2001), and their cortical axonal projections spread across multiple cortical columns (Ohno et al., 2012; Wimmer et al., 2010). These findings have led to the hypothesis of separate, parallel streams of sensory input to cortex (Bureau et al., 2006; Kim and Ebner, 1999; Yu et al., 2006), but because of anatomical and functional mixing of the pathways at both subcortical and

cortical levels, this proposal remains controversial (Veinante and Deschênes, 1999; Veinante et al., 2000; Feldmeyer, 2012).

Multi-whisker receptive fields in layer 2 fosGFP$^+$ neurons could be generated by direct thalamic input from widespread layer 1 POm axons and/or by barrel-targeted VPM input spread via cortico-cortical interactions (Fox et al., 2003; Goldreich et al., 1999). The presence of short latency spikes in POm (Figure S5) (Ahissar et al., 2000; Diamond et al., 1992; Masri et al., 2008; Sosnik et al., 2001), as well POm optogenetic stimulation (Figure 7) (Gambino et al., 2014), suggests that layer 2 neurons receive direct synaptic input from POm and that POm input may be sufficient to drive the short latency and broad receptive field responses observed in these cells during multi-whisker stimulation. While VPM neurons project to the barrel column center, POm neurons instead project to septal regions between barrels in rats (Wimmer et al., 2010). FosGFP$^+$ neurons could therefore be associated with septal circuits; however, fosGFP$^+$ neurons did not show distinct clustering in septal regions, and functional imaging in mice has shown that supragranular septal neurons are scattered throughout layer 2 (Bureau et al., 2006). Anatomical location of fosGFP$^+$ cells is therefore likely not a good indicator of paralemniscal circuits in mice.

Single-whisker stimulation of surrounding whiskers induces a latency and amplitude difference between fosGFP$^+$ and fosGFP$^-$ neurons. This result implies that VPM inputs from surrounding whiskers also contribute to surround responses in fosGFP$^+$ neurons. Future experiments should now use fosGFP as a marker to unravel the thalamo-cortical wiring underlying broad receptive field neurons in cortex with a combination of thalamic recordings, selective optogenetic inactivation of POm and VPM during single- and multi-whisker stimulation, and barrel-targeted cortical stimulation of ChR2-expressing thalamic axons.

Activity-Dependent Gene Expression Discriminates Sensory Response Properties

Here we used expression of an activity-dependent fluorescent reporter gene to differentiate between the receptive field properties of layer 2 neurons. Can these data help us understand what stimulus triggers reporter gene

expression in vivo? Although the prior stimulus that activated fosGFP expression in S1 is difficult to determine, multiple whisker stimulation is likely to be a common form of whisker stimulation during the first 2-3 weeks of life. Moreover, the extra synaptic input due to the broad receptive field input might explain in part why these neurons exhibit activity-dependent gene expression and have higher spontaneous (Yassin et al., 2010) and airpuff-evoked firing rates (Figures 3 and S2).

The preferred sensory input that most effectively drives firing in barrel cortex neurons, especially in supragranular layers, remains an open question. Barrel cortex layer 2/3 neurons have been functionally categorized by many stimulus response parameters including direction preference, stimulus frequency and phase locking, and single- versus multi-whisker preference (Andermann and Moore, 2006; Brecht et al., 2003; Estebanez et al., 2012; Ewert et al., 2008; Kremer et al., 2011; Simons, 1978). Our data suggest that broad receptive field, multi-whisker stimuli are effective drivers of spiking and activity-dependent gene expression during mouse development. Using single- or multi-whisker stimulation to drive fosGFP expression during sensory perception tasks could be a useful tool to investigate the formation of cortical cell assemblies with related sensory response properties.

Are fosGFP+ Neurons a Stable Subpopulation of Cortical Excitatory Neurons?

It has been proposed that there are a number of subtypes of excitatory neuron within cortical layer 2/3 (Feldmeyer, 2012); however, the lack of molecular markers for within-layer excitatory neuron subtypes has impeded efforts to uncover cortical sub-circuits and the synaptic mechanisms that underlie perception and behavior. Recently, axonal projection targets have been used to differentiate between layer 2/3 barrel cortex pyramidal neurons in behaving mice (Chen et al., 2013; Yamashita et al., 2013). Here we used fosGFP as a marker for layer 2/3 pyramidal neurons, which appear to project with similar likelihood to M1, S2, and contralateral S1 (Figure S4). This is consistent with the possibility that the fosGFP^{+} population does not consist of a molecularly specified population but is assembled by input competition. Furthermore, our inability to identify an anatomical correlate indicates that broad receptive field

input to layer 2/3 will drive activity in multiple downstream cortical targets. It remains possible that there are molecular markers that predict the emergence of the fosGFP population, but they could arise during early developmental periods. Future experiments investigating cell-type-specific gene expression and viral tracing of fosGFP neuron synaptic connectivity in vivo may help elucidate this point.

Are the receptive field response properties intrinsic to an identified subset of neurons or are they the result of plastic changes in developmentally unspecified excitatory cell networks? While levels of fosGFP are likely to change over the lifetime of a mouse, recent studies show that firing rates in individual cortical neurons can be stable over weeks (Cohen et al., 2013; Margolis et al., 2012). Therefore, fosGFP$^+$ neurons could be a stable population of neurons that overlaps with multi-whisker-responsive cortical neurons identified using other techniques (Estebanez et al., 2012; Ghazanfar and Nicolelis, 1997; Sato and Svoboda, 2010). Alternatively, they may display a continuum of sensory response properties with narrow and broad receptive field neurons at either end of the distribution (Elstrott et al., 2014). To distinguish between these possibilities, it will be necessary to perform long-term functional optical recordings of fosGFP$^+$ expressing neurons together with the identification of more stable anatomical or molecular markers that selectively label subsets of excitatory neurons.

Functional consequences

Multiple whisker stimulation is a commonly encountered form of sensory input. Our work provides a platform to examine the coding principles, wiring, and plasticity underlying somatosensory processing with a salient sensory stimulus. It will be of great interest to record and manipulate the activity of fosGFP$^+$ neurons in awake mice performing a cortically dependent behavioral task to characterize their role in triggering network activity, sensory processing, and perception.

EXPERIMENTAL PROCEDURES

All experiments were carried out in accordance with German regulations on animal welfare and/or the US National Institutes of Health guidelines for animals care and were approved by the Berlin ethics and veterinary committee and/or the Carnegie Mellon IACUC committee.

Surgery and Intrinsic Optical Imaging

P18 to P27 heterozygous fosGFP transgenic mice (Barth et al., 2004) were urethane- (1.5 g/kg) or isoflurane- anesthetized (1 to 2 %) to implant a light weight metal head holder to the skull with cyanoacrylate glue (Loctite 401) and a recording chamber from dental cement (Paladur). All recordings were made under urethane anesthesia only. Mouse body temperature was maintained at 37˚C with a heating blanket. In some experiments intrinsic optical imaging was performed to identify a specific barrel column. Briefly, the skull was illuminated with red light (630 nm) while a single whisker was deflected at 10 Hz for 5 s and images were collected with a cooled monochrome CCD camera (Q-Imaging). This manipulation did not induce fosGFP expression within the time window of the experiment. A small craniotomy (<1 mm) was made over the barrel column of interest after imaging or at stereotactic coordinates –1.2 mm posterior / 3.5 mm lateral to bregma and the dura was carefully removed to enable electrode entry.

Two-Photon Microscopy

Mice were placed under a two-photon laser scanning microscope (Femtonics) and the region of interest was scanned with a mode-locked Ti:sapphire laser beam (Ultra 1, Coherent) using a 40 x 0.8 NA water immersion objective (Olympus). Two or three recording electrodes containing Alexa-594 (Invitrogen) were inserted into the brain with positive pressure. Photons emitted by the Alexa-594 under 820nm light excitation were detected using a non-descanned photomultiplier tube (PMT) and revealed dark shadows in live tissue identifying somata within the neuropil. A second PMT was used to identify $fosGFP^{+}$ neurons using 930 nm wavelength laser stimulation. Sequential images were made from the same optical section to target

pyramidal-like cell somata of fosGFP$^+$ and fosGFP$^-$ excitatory neurons. We visually selected fosGFP$^+$ and fosGFP$^-$ cells during an experiment using their fluorescence signal. In each experiment, cells were positively identified as excitatory neurons from z stack images of the Alexa-594-filled cells, made using a series of optical sections separated by 3 µm.

Electrophysiology

Whole-cell patch clamp recordings were made with 5-7 mOhms, 2 mm external diameter borosilicate glass (Hiligenberg) pipettes and filled with intracellular recording solution containing, in mM, the following: 135 K-gluconate, 4 KCl, 10 HEPES, 10 phosphocreatine, 4 MgATP, 0.3 Na_3GTP (adjusted to pH 7.3 with KOH), 2 mg/ml biocytin, and 30 µm Alexa-594 (Invitrogen). The brain was covered with Ringer's solution containing, in mM, the following: 135 NaCl, 5 KCl, 5 HEPES, 1.8 $CaCl_2$, and 1 $MgCl_2$. An Ag/AgCl ground electrode was placed in the recording chamber and two or three whole-cell pipettes were inserted into the brain under visual control. Electrodes were positioned at an oblique angle (47° from vertical) at the surface and moved approximately 100 µm into the brain with 130-150 mbar pressure to ensure the electrode tip was clear, using motorized micromanipulators (Luigs and Neumann). Pressure was then decreased to 50 mbar and electrodes positioned in layer 2 that was visible as a dense layer of somata underneath the cell-sparse layer 1. Pyramidal-like cell somata were targeted for recording using the shadow-patching technique (Kitamura et al., 2008). Cells of interest were carefully approached at low positive pressure (30 mbar). Resistance changes signifying contact with a neuron were visually identified on a TDS2024C oscilloscope (Tektronix). Upon contact, negative pressure was applied to form a gigaseal and establish the whole-cell configuration in voltage clamp mode. Current clamp-recordings were then made using an Axon Multiclamp 700B amplifier (Molecular Devices). Recordings were digitized at 20 kHz by ITC-18 (Heka), high-pass filtered at 10 kHz, and collected in 60 s sweeps using custom macros written in IgorPro (Wavemetrics). Recordings were only included in the data set if the mean Downstate membrane potential was < –50 mV. The liquid junction potential was not compensated. Immediately after break-in, firing patterns were

examined with current injection (–200 to 300 pA in 100 pA steps), and only cells with adapting firing patterns and broad action potentials were included for analysis.

Whisker Stimulation

For airpuff stimulation, all whiskers were intact. Airpuff stimuli were delivered through a plastic tube of 3 mm diameter 5 cm away from the whisker pad via a solenoid valve (Research Incorporated; 20 psi) controlled by IgorPro at 0.25 Hz. In a subset of experiments, the latency of puff-driven whisker movements was verified using high-speed (500 Hz) filming (Genie, Imaging Solutions GmbH), and the time difference between the command pulse and whisker deflection, typically 10 ms, was corrected during analysis. All latencies reported are therefore from whisker movement onset, not from the command pulse. For single-whisker stimulation, all whiskers except the principal whisker were trimmed to about 3 mm length. The principal whisker (C2) and sometimes a surrounding whisker (B2) were then placed in thin glass tubes glued to a piezoelectric bimorph. Rostro-caudal 500-800 µm (calibrated with high-speed filming) whisker movements were driven by a brief (1 ms) current pulses delivered to the piezo at 0.25 Hz.

Histology and Cell Identification

Cell identification was assessed in vivo after the cells had been filled with the intracellular solution containing the fluorescent dye Alexa 594 and confirmed post hoc using revelation of biocytin. Following recordings, mice were transcardially perfused with 0.1 M PBS followed by 4 % paraformaldehyde (PFA) in PBS. The brain was then removed, immersed in 4 % PFA overnight at 4 ˚C, and stored in PBS before histological processing. The brain was sliced into 100 µm thick tangential or, for experiments involving viral infections, thalamocortical sections using a Leica VT1000 S vibratome. Barrels were identified using cytochrome oxidase staining and recorded cells filled with biocytin revealed using ABC kit Vectastain (Vector). Slices were mounted in Moviol and stored at 4 ˚C. Neurons were photographed and reconstructed with Neurolucida software (Micro Bright Field Bioscience).

Virus-Mediated ChR2 Expression and Optical Stimulation

A lentivirus encoding ChR2-eYFP (VSVG.HIV.SIN.Synapsin.ChR2 (H134R).EYFP.WP; Addgene 20945) (Zhang et al., 2007) was injected in P10 to P12 animals. Briefly, the mouse was anesthetized with intraperitoneal injection of ketamine (100 mg/kg), xylazine (5 mg/kg), and acepromazine (3 mg/kg). Next, animals were placed in a computerized stereotactic frame (Angle Two, Leica). A small craniotomy was performed over the POm with coordinates –1.8 mm posterior, 1.25 mm lateral to Bregma or VPM coordinates –1.8 mm posterior, and 1.75 mm lateral to Bregma. A glass injection pipette with 10 µm diameter tip containing lentivirus was then inserted to a depth of 2.75 mm below the brain surface for POm or 3.25 mm for VPM. Using an oil piston (MO-10; Narishige) connected to this injection glass pipette 0.5 to 0.6 µl of virus was injected at a rate of 50 to 100 nl per minute. The injection pipette stayed in place for about 10 min to allow the pressure to equilibrate after the injection and then removed slowly.

Recordings were carried out 1 to 2 weeks following virus injection. On the day of the experiment, a second craniotomy was made over the contralateral hemisphere to the recording (–1.8 mm posterior; 2 mm lateral) for insertion of the fiber optic (200 µm diameter; Thor Labs) coupled to a 450-480 nm blue light source (473 nm DPSS Laser System; LabSpec) into the POm. A 3 ms light pulse (~40 mW) was delivered at 0.25 Hz controlled by IgorPro. Post hoc, all infection sites were verified for VPM with a characteristic L5B and L4 axonal projection pattern and POm with a characteristic L5A and L1 axonal projection pattern. Electrophysiological data from animals with infection sites that overlapped the POm and VPM boundary or had mixed VPM and POm-like cortical axonal projections patterns were discarded.

Data analysis

Data analysis was carried out for individual cells within each pair using IgorPro. The fluorescence signal of the fosGFP$^+$ cell was normalized to the brightest cell in the field of view and fosGFP$^+$ cells were selected using a threshold value of 0.4 (Figure S1). Two-tailed Wilcoxon signed rank tests were used to test for significance. All data are plotted as the mean ± SEM. N numbers are the number of pairs of fosGFP$^+$ / fosGFP$^-$ neurons unless

otherwise stated. In one experiment we recorded three neurons simultaneously: two fosGFP$^+$ neurons and one fosGFP$^-$ neuron. This was included in the dataset as two pairs of fosGFP$^+$ / fosGFP$^-$ neurons.

Analysis of Sensory Responses in Downstates

Because of large and variable V_m changes during Upstates, analysis focused on whisker-evoked responses during the hyperpolarized Downstate. Downstates were identified by a hyperpolarized V_m that showed little change (<3 mV) during a 50 ms window immediately preceding the stimulus. Between 8 and 56 Downstate stimulus epochs were analyzed per cell pair. All selected segments were visually inspected and averaged to determine response latency, amplitude, integral, and onset slope of response. Because state transitions were highly correlated between cells in the recorded pair (i.e., both cells were simultaneously in Up- or Down-states), selection analysis on one cell was sufficient to identify Downstate trace segments for both cells in the pair. SEM plotted around the averaged traces was calculated after subtraction of prestimulus V_m.

Latency

To compare the latency of the subthreshold response between pairs, V_m for the time period –10 to –7 ms before stimulus onset was calculated, and the standard deviation (SD_{-10ms}) was determined. A running average (1 ms bins) for the entire averaged segment trace for that cell was calculated. Onset response latency was identified as when the standard deviation (SD_{1msbin}) of the averaged V_m was three times the SD_{-10ms}. All latency measurements were visually inspected and verified.

Amplitude

The amplitude of the sensory response was determined by subtracting the baseline V_m from the peak response. The baseline was calculated as the mean V_m from 5 to 6 ms poststimulus for airpuff stimuli and the mean V_m from 5 to 4 ms prestimulus for piezo and the optogenetic stimulation, times when we never saw any evidence of an evoked response. The peak response was measured as the mean V_m at 1 ms around the time of the peak response

identified within the first 30 ms of the sensory or optogenetic response for both fosGFP^{+} and fosGFP^{-} neurons.

Onset Slope

The rate of rise of the evoked synaptic response, or onset slope, was measured by a linear fit between 20 and 80 % of the peak response amplitude.

ACKNOWLEDGEMENTS

We would like to thank Janett König for technical assistance and Prof. Imre Vida for advice on cell reconstruction and use of his NeuroLucida system. We thank Birgit Voigt, Nevena Milenkovic, Evgeny Bobrov, D.J. Brasier, Erika Fanselow, Joanna Urban-Ciecko for critical comments on earlier versions of the manuscript. This work was funded by grants from the Deutsche Forschungs gemeinschaft (Exc 257 NeuroCure and BaCoFun, JFAP), a European Research Council starting grant (ERC-2010-StG-260590, JFAP), the Alexander von Humboldt Foundation (ALB), the European Union (FP7 3x3Dimaging 323945, JFAP) and NIH (DA 0171-88) (ALB).

REFERENCES

Adesnik, H., Bruns, W., Taniguchi, H., Huang, Z.J., and Scanziani, M. (2012). A neural circuit for spatial summation in visual cortex. Nature *490*, 226–231.

Ahissar, E., Sosnik, R., and Haidarliu, S. (2000). Transformation from temporal to rate coding in a somatosensory thalamocortical pathway. Nature *406*, 302–306.

Andermann, M.L., and Moore, C.I. (2006). A somatotopic map of vibrissa motion direction within a barrel column. Nat. Neurosci. *9*, 543–551.

Anderson, C.T., Sheets, P.L., Kiritani, T., and Shepherd, G.M.G. (2010). Sublayer-specific microcircuits of corticospinal and corticostriatal neurons in motor cortex. Nat. Neurosci. *13*, 739–744.

Barth, A.L., and Poulet, J.F.A. (2012). Experimental evidence for sparse firing in the neocortex. Trends in Neurosciences *35*, 345–355.

Barth, A.L., Gerkin, R.C., and Dean, K.L. (2004). Alteration of neuronal firing properties after in vivo experience in a FosGFP transgenic mouse. J. Neurosci. *24*, 6466–6475.

Benedetti, B.L., Takashima, Y., Wen, J.A., Urban-Ciecko, J., and Barth, A.L. (2013). Differential wiring of layer 2/3 neurons drives sparse and reliable firing during neocortical development. Cereb. Cortex *23*, 2690–2699.

Boyden, E.S., Zhang, F., Bamberg, E., Nagel, G., and Deisseroth, K. (2005). Millisecond-timescale, genetically targeted optical control of neural activity. Nat. Neurosci. *8*, 1263–1268.

Brecht, M., and Sakmann, B. (2002). Dynamic representation of whisker deflection by synaptic potentials in spiny stellate and pyramidal cells in the barrels and septa of layer 4 rat somatosensory cortex. J. Physiol. (Lond.) *543*, 49–70.

Brecht, M., Roth, A., and Sakmann, B. (2003). Dynamic receptive fields of reconstructed pyramidal cells in layers 3 and 2 of rat somatosensory barrel cortex. J. Physiol. (Lond.) *553*, 243–265.

Brown, S.P., and Hestrin, S. (2009). Intracortical circuits of pyramidal neurons reflect their long-range axonal targets. Nature *457*, 1133–1136.

Bureau, I., Saint Paul, von, F., and Svoboda, K. (2006). Interdigitated paralemniscal and lemniscal pathways in the mouse barrel cortex. PLoS Biol. *4*, e382.

Carandini, M., and Ferster, D. (2000). Membrane potential and firing rate in cat primary visual cortex. J. Neurosci. *20*, 470–484.

Carvell, G.E., and Simons, D.J. (1990). Biometric analyses of vibrissal tactile

discrimination in the rat. J. Neurosci. *10*, 2638–2648.

Chen, J.L., Carta, S., Soldado-Magraner, J., Schneider, B.L., and Helmchen, F. (2013). Behaviour-dependent recruitment of long-range projection neurons in somatosensory cortex. Nature *499*, 336–340.

Chiaia, N.L., Rhoades, R.W., Fish, S.E., and Killackey, H.P. (1991). Thalamic processing of vibrissal information in the rat: II. Morphological and functional properties of medial ventral posterior nucleus and posterior nucleus neurons. J. Comp. Neurol. *314*, 217–236.

Cohen, L., Koffman, N., Meiri, H., Yarom, Y., Lampl, I., and Mizrahi, A. (2013). Time-lapse electrical recordings of single neurons from the mouse neocortex. Proc. Natl. Acad. Sci. U.S.a. *110*, 5665–5670.

Crochet, S., Poulet, J.F.A., Kremer, Y., and Petersen, C.C.H. (2011). Synaptic mechanisms underlying sparse coding of active touch. Neuron *69*, 1160–1175.

Diamond, M.E., Armstrong-James, M., and Ebner, F.F. (1992). Somatic sensory responses in the rostral sector of the posterior group (POm) and in the ventral posterior medial nucleus (VPM) of the rat thalamus. J. Comp. Neurol. *318*, 462–476.

Elstrott, J., Clancy, K.B., Jafri, H., Akimenko, I., and Feldman, D.E. (2014). Cellular mechanisms for response heterogeneity among L2/3 pyramidal cells in whisker somatosensory cortex. J. Neurophysiol. *112*, 233–248.

Estebanez, L., Boustani, El, S., Destexhe, A., and Shulz, D.E. (2012). Correlated input reveals coexisting coding schemes in a sensory cortex. Nat. Neurosci. *15*, 1691–1699.

Ewert, T.A.S., Vahle-Hinz, C., and Engel, A.K. (2008). High-frequency whisker vibration is encoded by phase-locked responses of neurons in the rat's barrel cortex. J. Neurosci. *28*, 5359–5368.

Feldmeyer, D. (2012). Excitatory neuronal connectivity in the barrel cortex. Front Neuroanat *6*, 24.

Fox, K., Wright, N., Wallace, H., and Glazewski, S. (2003). The origin of cortical surround receptive fields studied in the barrel cortex. J. Neurosci. *23*, 8380–8391.

Friedberg, M.H., Lee, S.M., and Ebner, F.F. (1999). Modulation of receptive field properties of thalamic somatosensory neurons by the depth of anesthesia. J. Neurophysiol. *81*, 2243–2252.

Gambino, F., Pagès, S., Kehayas, V., Baptista, D., Tatti, R., Carleton, A., Holtmaat, A., Sensory-evoked LTP driven by dendritic plateau potentials in vivo. Nature doi:10.1038/nature13664.

Gentet, L.J., Kremer, Y., Taniguchi, H., Huang, Z.J., Staiger, J.F., and

Petersen, C.C.H. (2012). Unique functional properties of somatostatin-expressing GABAergic neurons in mouse barrel cortex. Nat. Neurosci. *15*, 607–612.

Ghazanfar, A.A., and Nicolelis, M.A. (1997). Nonlinear processing of tactile information in the thalamocortical loop. J. Neurophysiol. *78*, 506–510.

Goldreich, D., Kyriazi, H.T., and Simons, D.J. (1999). Functional independence of layer IV barrels in rodent somatosensory cortex. J. Neurophysiol. *82*, 1311–1316.

Haider, B., and McCormick, D.A. (2009). Rapid neocortical dynamics: cellular and network mechanisms. Neuron *62*, 171–189.

Higley, M.J., and Contreras, D. (2003). Nonlinear integration of sensory responses in the rat barrel cortex: an intracellular study in vivo. J. Neurosci. *23*, 10190–10200.

Hofer, S.B., Ko, H., Pichler, B., Vogelstein, J., Ros, H., Zeng, H., Lein, E., Lesica, N.A., and Mrsic-Flogel, T.D. (2011). Differential connectivity and response dynamics of excitatory and inhibitory neurons in visual cortex. Nat. Neurosci. *14*, 1045–1052.

Kerlin, A.M., Andermann, M.L., Berezovskii, V.K., and Reid, R.C. (2010). Broadly tuned response properties of diverse inhibitory neuron subtypes in mouse visual cortex. Neuron *67*, 858–871.

Kim, U., and Ebner, F.F. (1999). Barrels and septa: separate circuits in rat barrels field cortex. J. Comp. Neurol. *408*, 489–505.

Kitamura, K., Judkewitz, B., Kano, M., Denk, W., and Häusser, M. (2008). Targeted patch-clamp recordings and single-cell electroporation of unlabeled neurons in vivo. Nat. Methods *5*, 61–67.

Ko, H., Hofer, S.B., Pichler, B., Buchanan, K.A., Sjöström, P.J., and Mrsic-Flogel, T.D. (2011). Functional specificity of local synaptic connections in neocortical networks. Nature *473*, 87–91.

Koralek, K.A., Jensen, K.F., and Killackey, H.P. (1988). Evidence for two complementary patterns of thalamic input to the rat somatosensory cortex. Brain Res. *463*, 346–351.

Kremer, Y., Léger, J.-F., Goodman, D., Brette, R., and Bourdieu, L. (2011). Late emergence of the vibrissa direction selectivity map in the rat barrel cortex. J. Neurosci. *31*, 10689–10700.

Kuhlman, S.J., Tring, E., and Trachtenberg, J.T. (2011). Fast-spiking interneurons have an initial orientation bias that is lost with vision. Nat. Neurosci. *14*, 1121–1123.

Lampl, I., Reichova, I., and Ferster, D. (1999). Synchronous membrane potential fluctuations in neurons of the cat visual cortex. Neuron *22*, 361–374.

Lu, S.M., and Lin, R.C. (1993). Thalamic afferents of the rat barrel cortex: a light- and electron-microscopic study using Phaseolus vulgaris leucoagglutinin as an anterograde tracer. Somatosens Mot Res *10*, 1–16.

Margolis, D.J., Lütcke, H., Schulz, K., Haiss, F., Weber, B., Kügler, S., Hasan, M.T., and Helmchen, F. (2012). Reorganization of cortical population activity imaged throughout long-term sensory deprivation. Nat. Neurosci. *15*, 1539–1546.

Masri, R., Bezdudnaya, T., Trageser, J.C., and Keller, A. (2008). Encoding of Stimulus Frequency and Sensor Motion in the Posterior Medial Thalamic Nucleus. J. Neurophysiol. *100*, 681–689.

Moore, C.I., and Nelson, S.B. (1998). Spatio-temporal subthreshold receptive fields in the vibrissa representation of rat primary somatosensory cortex. J. Neurophysiol. *80*, 2882–2892.

Nicolelis, M.A., Lin, R.C., Woodward, D.J., and Chapin, J.K. (1993). Dynamic and distributed properties of many-neuron ensembles in the ventral posterior medial thalamus of awake rats. Proc. Natl. Acad. Sci. U.S.a. *90*, 2212–2216.

Oberlaender, M., Ramirez, A., and Bruno, R.M. (2012). Sensory experience restructures thalamocortical axons during adulthood. Neuron *74*, 648–655.

Ohno, S., Kuramoto, E., Furuta, T., Hioki, H., Tanaka, Y.R., Fujiyama, F., Sonomura, T., Uemura, M., Sugiyama, K., and Kaneko, T. (2012). A morphological analysis of thalamocortical axon fibers of rat posterior thalamic nuclei: a single neuron tracing study with viral vectors. Cereb. Cortex *22*, 2840–2857.

Okun, M., and Lampl, I. (2008). Instantaneous correlation of excitation and inhibition during ongoing and sensory-evoked activities. Nat. Neurosci. *11*, 535–537.

Perin, R., Berger, T.K., and Markram, H. (2011). A synaptic organizing principle for cortical neuronal groups. Proc. Natl. Acad. Sci. U.S.a. *108*, 5419–5424.

Pierret, T., Lavallée, P., and Deschênes, M. (2000). Parallel streams for the relay of vibrissal information through thalamic barreloids. J. Neurosci. *20*, 7455–7462.

Poulet, J.F.A., and Petersen, C.C.H. (2008). Internal brain state regulates membrane potential synchrony in barrel cortex of behaving mice. Nature *454*, 881–885.

Rhoades, R.W., Belford, G.R., and Killackey, H.P. (1987). Receptive-field properties of rat ventral posterior medial neurons before and after selective kainic acid lesions of the trigeminal brain stem complex. J. Neurophysiol. *57*, 1577–1600.

Runyan, C.A., Schummers, J., Van Wart, A., Kuhlman, S.J., Wilson, N.R.,

Huang, Z.J., and Sur, M. (2010). Response features of parvalbumin-expressing interneurons suggest precise roles for subtypes of inhibition in visual cortex. Neuron *67*, 847–857.

Sato, T.R., and Svoboda, K. (2010). The functional properties of barrel cortex neurons projecting to the primary motor cortex. J. Neurosci. *30*, 4256–4260.

Simons, D.J. (1978). Response properties of vibrissa units in rat SI somatosensory neocortex. J. Neurophysiol. *41*, 798–820.

Simons, D.J., and Carvell, G.E. (1989). Thalamocortical response transformation in the rat vibrissa/barrel system. J. Neurophysiol. *61*, 311–330.

Song, S., Sjöström, P.J., Reigl, M., Nelson, S., and Chklovskii, D.B. (2005). Highly nonrandom features of synaptic connectivity in local cortical circuits. PLoS Biol. *3*, e68.

Sosnik, R., Haidarliu, S., and Ahissar, E. (2001). Temporal Frequency of Whisker Movement. I. Representations in Brain Stem and Thalamus. J. Neurophysiol. *86*, 339–353.

Varga, Z., Jia, H., Sakmann, B., and Konnerth, A. (2011). Dendritic coding of multiple sensory inputs in single cortical neurons in vivo. Proc. Natl. Acad. Sci. U.S.a. *108*, 15420–15425.

Veinante, P., and Deschênes, M. (1999). Single- and multi-whisker channels in the ascending projections from the principal trigeminal nucleus in the rat. J. Neurosci. *19*, 5085–5095.

Veinante, P., Jacquin, M.F., and Deschênes, M. (2000). Thalamic projections from the whisker-sensitive regions of the spinal trigeminal complex in the rat. J. Comp. Neurol. *420*, 233–243.

Waite, P.M. (1973). Somatotopic organization of vibrissal responses in the ventro-basal complex of the rat thalamus. J. Physiol. (Lond.) *228*, 527–540.

Williams, M.N.M., Zahm, D.S.D., and Jacquin, M.F.M. (1994). Differential foci and synaptic organization of the principal and spinal trigeminal projections to the thalamus in the rat. Eur. J. Neurosci. *6*, 429–453.

Wimmer, V.C., Bruno, R.M., de Kock, C.P.J., Kuner, T., and Sakmann, B. (2010). Dimensions of a projection column and architecture of VPM and POm axons in rat vibrissal cortex. Cereb. Cortex *20*, 2265–2276.

Yamashita, T., Pala, A., Pedrido, L., Kremer, Y., Welker, E., and Petersen, C.C.H. (2013). Membrane potential dynamics of neocortical projection neurons driving target-specific signals. Neuron *80*, 1477–1490.

Yassin, L., Benedetti, B.L., Jouhanneau, J.-S., Wen, J.A., Poulet, J.F.A., and Barth, A.L. (2010). An Embedded Subnetwork of Highly Active Neurons in the Neocortex. Neuron *68*, 1043–1050.

Yoshimura, Y., Dantzker, J.L.M., and Callaway, E.M. (2005). Excitatory cortical neurons form fine-scale functional networks. Nature *433*, 868–873.

Yu, C., Derdikman, D., Haidarliu, S., and Ahissar, E. (2006). Parallel thalamic pathways for whisking and touch signals in the rat. PLoS Biol. *4*, e124.

Yu, J., and Ferster, D. (2010). Membrane potential synchrony in primary visual cortex during sensory stimulation. Neuron *68*, 1187–1201.

Zhang, F., Wang, L.-P., Brauner, M., Liewald, J.F., Kay, K., Watzke, N., Wood, P.G., Bamberg, E., Nagel, G., Gottschalk, A., et al. (2007). Multimodal fast optical interrogation of neural circuitry. Nature *446*, 633–639.

Zhu, J.J., and Connors, B.W. (1999). Intrinsic firing patterns and whisker-evoked synaptic responses of neurons in the rat barrel cortex. J. Neurophysiol. *81*, 1171–1183.

FIGURE LEGENDS

Figure 1. Single Principal Whisker Stimulation Triggers a Similar Early Synaptic Response in fosGFP$^+$ and fosGFP$^-$ Neurons.

(A) Schematic of piezo-driven glass rod (shaded gray) deflecting a single principal whisker (C2, bold red) and two-photon targeted dual whole-cell recordings in the C2 barrel column.

(B) Partial reconstruction within the barrel map of a fosGFP$^+$ (green) fosGFP$^-$ (black) cell pair confirms C2 targeting.

(C) Four single trial responses to piezo-driven C2 whisker deflection. V_m mark fosGFP$^+$ / fosGFP$^-$ (mV) from top to bottom: –63.5 / –58.3; –63.6 / –57.0; –60.8 / –58.7; –62.4 / –56.8.

(D) Trial-by-trial measurements of latency from the pair in (C) (n = 27 trials) shows no differences in latency.

(E) Averaged subthreshold response to piezo stimulation for the pair of cells shown in (C). SEM is shown in shaded color around the mean. V_m mark fosGFP$^+$ / fosGFP$^-$ (mV): –61.9 / –56.2.

(F) Four single trial responses to piezo-driven C2 whisker deflection from the reconstructed pair in (B). V_m mark fosGFP$^+$ / fosGFP$^-$ (mV) from top to bottom: –64.9 / –60.7; –65.3 / –64.1; –64.6 / –60.3; –63.9 / –61.7.

(G) Trial-by-trial measurements of latency for the pair shown in (F) show no differences in the latency of the fosGFP$^+$ neuron compared to the fosGFP$^-$ (n = 20 trials).

(H) Averaged subthreshold response to piezo stimulation to the pair of cells in (F). SEM is represented in shaded color around the mean. V_m mark fosGFP$^+$ / fosGFP$^-$ (mV): –65.3 / –62.7.

(I-K) FosGFP$^+$ and fosGFP$^-$ neurons show no significant differences in the (I) latency, (J) amplitude, and (K) onset slope of the early synaptic response to brief deflection of the principal whisker (n = 17 pairs). Light gray and dark gray circles correspond to example neurons in (C) and (F) respectively. Red filled circles with error bars show mean ± SEM.

(L) Population average of the synaptic response to principal whisker stimulation in neighboring fosGFP$^+$ and fosGFP$^-$ neurons (n = 17 pairs).

Shaded background shows the SEM of the baseline-subtracted synaptic responses. V_m mark fosGFP$^+$ / fosGFP$^-$ (mV): -61.4 / -61.0.

Figure 2. FosGFP$^+$ Neurons Respond with Shorter Latency and Larger Amplitude Synaptic Responses to Airpuff Deflection of Multiple Whiskers.

(A) Schematic of dual two-photon targeted whole-cell recording setup to investigate sensory processing in neighboring barrel cortex fosGFP$^+$ and fosGFP$^-$ excitatory neurons. Blue circle represents airpuff stimulation.

(B) Left, in vivo two-photon image of a pair of fosGFP$^+$ and fosGFP$^-$ neurons recorded and filled with Alexa-594. Right, short sections of in vivo images of the dendrites of the same cells showing spines in (top) fosGFP$^-$ and (bottom) fosGFP$^+$ neurons. Scale bar left, 30 µm, and right, 5 µm.

(C) Four single trial sensory responses to airpuff stimulation from the pair shown in (B) showing larger amplitude and shorter latency in the fosGFP$^+$ neuron. V_m mark fosGFP$^+$ / fosGFP$^-$ (mV) from top to bottom: –58.0 / –61.7; -58.9 / –61.5; –61.5 / –61.5; –61.1 / –60.7.

(D) Trial-by-trial latency measurements from this example pair show stable latency in the fosGFP$^+$ neuron but variable, longer latencies in the fosGFP$^-$ neuron to airpuff stimulation (n = 16 trials).

(E) Averaged sensory response from same pair of cells 0 to 30 ms after multi-whisker deflection with an airpuff. V_m mark fosGFP$^+$ / fosGFP$^-$ (mV): –60.1 / –61.1. Shaded background is the SEM.

(F-H) Population data (n = 10) show that fosGFP$^+$ neurons have a (F) significantly shorter latency, (G) larger amplitude, and (H) faster slope of the initial evoked subthreshold response to airpuff stimulation. Gray filled circles correspond to pair in (C-E). Red circles with error bars show mean ± SEM.

(I) Average of the synaptic response from the entire dataset with SEM shown as shaded background (n = 10). V_m mark fosGFP$^+$ / fosGFP$^-$ (mV): -62.9/ -60.1.

Figure 3. Prolonged Sensory Response Following Multiple Whisker Airpuff Stimulation Triggers More Action Potentials in fosGFP$^+$ than fosGFP$^-$ Neurons.

(A) Example single-trial dual whole-cell V_m recordings during whisker stimulation in cortical Downstates showing synchronous, large-amplitude prolonged sensory responses in both neurons. Action potentials have been truncated. V_m mark fosGFP$^+$ / fosGFP$^-$ (mV) from top to bottom: –58.0 / –61.7; –58.9 / –61.5; –61.5 / –61.5; –61.1 / –60.7.

(B) For the same recordings, the averaged sensory response from 16 trials aligned to whisker deflection onset. V_m mark fosGFP$^+$ / fosGFP- (mV): –60.1 / –61.1.

(C) Population peristimulus time histogram (PSTH) of action potential firing calculated for ten pairs of neurons with fosGFP$^+$ in green and fosGFP$^–$ in gray, bin size 100 ms.

(D) The mean number of action potentials (APs) fired in the 0 to 1.5 s post-stimulus onset was significantly greater in fosGFP$^+$ than fosGFP$^–$ neurons. Red filled circle with error bars shows mean ± SEM.

(E) The charge transfer (integral) of the V_m 0 to 2 s poststimulus was larger in fosGFP$^+$ than fosGFP$^–$ neurons. Red filled circles with error bars show mean ± SEM. The recording in (A) and (B) is from the same cell pair and shows the same stimulus trials as shown in Figure 2C and 2D. Gray filled circles in (D) and (E) indicate data from pair in (A) and (B).

Figure 4. Multi-Whisker Stimulation Directed to the Central Whisker Row Triggers a Similar Synaptic Response in fosGFP$^+$ and fosGFP$^–$ Neurons.

(A) Schematic of the setup for airpuff stimulation directed to C row during dual two-photon targeted whole cell recordings from C row; a single C row whisker is colored in bold red.

(B) Partial reconstruction within the barrel map of a fosGFP$^+$ (green) / fosGFP$^–$ (black) cell pair confirms C row targeting.

(C) Four single trial responses to airpuff stimulation towards the C row. V_m mark fosGFP$^+$ / fosGFP$^–$ (mV) from top to bottom: –62.9 / –64.4; –63.8 / –65.9; –64.0 / –66.3; –65.8 / –67.7.

(D) Trial-by-trial measurements of latency in the same pair of cells show similar latencies across trials between fosGFP$^+$ and fosGFP$^–$ neurons (n = 30 trials).

(E) Averaged sensory response from the same pair of cells 0 to 30 ms after multi-whisker deflection with an airpuff stimulus. V_m mark fosGFP$^+$ / fosGFP$^-$ (mV): –64.9 / –66.8. Shaded background is the SEM.

(F-H) Population data (n = 7) show no significant differences in (F) latency, (G) amplitude, and (H) slope during central whisker targeted airpuff stimulation. Gray filled circles correspond to the pair in (C)-(E). Red circles with error bars show mean ± SEM.

(I) Average of the synaptic response from the entire dataset with central-whisker targeted airpuff stimulation with SEM shown as shaded background around the mean (n = 7). V_m mark fosGFP$^+$ / fosGFP$^-$ (mV): -64.1/ -64.5.

Figure 5. FosGFP$^+$ Neurons Are Targeted by Surround Multi-Whisker Stimulation.

(A) Schematic of the setup for airpuff stimulation directed towards the E row during dual two-photon targeted whole-cell recordings from cells in the A row; a single A row whisker is colored in bold red.

(B) Partial reconstruction within the barrel map of a fosGFP$^+$ (green) / fosGFP$^-$ (black) cell pair confirms A row targeting.

(C) Four single trial responses from same cells as in (B) to airpuff stimulation toward the E row. V_m mark fosGFP$^+$ / fosGFP$^-$ (mV) from top to bottom: –67.1 / –63.7; –67.0 / –64.6; –68.1 / –65.4; –66.6 / –64.2.

(D) Trial-by-trial measurements of latency from the pair in (C) show consistently earlier responses in fosGFP$^+$ neurons compared to fosGFP- neurons (n = 42 trials).

(E) Averaged sensory response from the same example pair of cells 0 to 30ms after multi-whisker deflection with an airpuff stimulus directed toward the E row. V_m mark fosGFP$^+$ / fosGFP$^-$ (mV): –67.1 / –64.1. Shaded background around the mean is the SEM.

(F-H) Analysis of eight dual recordings during surround whisker stimulation showing significantly (F) shorter response latency, (G) larger amplitude, and (H) faster onset slope in fosGFP$^+$ neurons as compared to fosGFP$^-$ neurons during surround multi-whisker stimulation. Gray filled circles correspond to the pair in (C)-(E). Red circles with error bars show mean ± SEM.

(I) Population average (n = 8) of the early synaptic response to surround airpuff stimulation of the whisker pad with shaded SEM. V_m mark fosGFP$^+$ / fosGFP$^-$ (mV): -62.3/ -60.3.

Figure 6. Single Surround Whisker Stimulation Targets fosGFP$^+$ Neurons.

(A) Schematic showing zoom of whisker pad with principal whisker (PW, red, C2 whisker) and surround whisker (SW, blue, B2 whisker) with piezo-driven glass rods attached.

(B) Partial reconstruction within the barrel map of a fosGFP$^+$ (green) / fosGFP$^-$ (black) cell pair confirming C2 barrel (shaded red) targeting and showing B2 (shaded blue) surround barrel.

(C) Four single trial responses to principal whisker C2 deflection from cells in (B). V_m mark fosGFP$^+$ / fosGFP$^-$ (mV) from top to bottom: –58.4 / –58.5; –60.0 / –59.0; –60.8 / –60.8; –61.4 / –61.5.

(D) Trial-by-trial measurements of latency in the pair shown in (C) (n = 22 trials) show no differences in the latency when stimulating the principal whisker between fosGFP$^+$ and fosGFP$^-$ neurons.

(E) Averaged subthreshold response to piezo stimulation of the pair of cells shown in (C) and (D). SEM is shown as shaded color around the mean. V_m mark fosGFP$^+$ / fosGFP$^-$ (mV): –57.3 / –58.1.

(F) Four single trial responses from the same pair of cells as in (B) and (C) to interleaved surround whisker B2 deflection. V_m mark fosGFP$^+$ / fosGFP$^-$ (mV) from top to bottom: –55.0 / –58.2; –59.3 / –59.9; –60.1 / –60.8; –61.3 / –61.5.

(G) Trial-by-trial measurements of latency from the pair in (F) show consistently earlier responses in fosGFP$^+$ neurons during surround whisker stimulation (n = 27 trials).

(H) Averaged subthreshold response to piezo stimulation for the pair of cells in (F-G). Shaded color around the mean is SEM. V_m mark fosGFP$^+$ / fosGFP$^-$ (mV): –58.1 / –58.7.

(I-K) Population analysis (n = 10) of the surround whisker deflection response shows a significantly (I) shorter response latency, (H) larger amplitude, and (K) faster onset slope in fosGFP$^+$ neurons compared to fosGFP$^-$ neurons.

Gray filled circles correspond to example pair in (C)-(H). Blue filled circles with error bars show mean ± SEM.

(L) Population average of the synaptic response to surround whisker stimulation in neighboring fosGFP$^+$ and fosGFP$^-$ neurons (n = 10 pairs). Shaded background around the mean shows SEM of the responses. V_m mark fosGFP$^+$ / fosGFP$^-$ (mV): -61.3/ -60.3.

Figure 7. Optogenetic Responses to VPM Stimulation Are Similar in fosGFP$^+$ and fosGFP$^-$ Neurons.

(A) Schematic of two-photon targeted dual recording setup with optical fiber (cyan) inserted into the VPM thalamic nucleus for ChR2 stimulation.

(B) Fluorescence image of a thalamocortical slice showing VPM ChR2-GFP infection site in the thalamus and axonal projections in cortex; white schematic outlines of the brain structures are from the same slice under bright field illumination. Scale bar, 1 mm.

(C) Four single trial responses to 3 ms blue light stimulation (cyan bar) of VPM corresponding to anatomy in (B). V_m mark fosGFP$^+$ / fosGFP- (mV) from top to bottom: –61.1 / –58.3; –64.7 / –61.8; –64.1 / –60.4; –60.8 / –58.8.

(D) Trial-by-trial measurements of latency in the pair shown in (C) show no difference in fosGFP$^+$ neurons compared to fosGFP$^-$ neurons (n = 22 trials).

(E) Averaged subthreshold response to ChR2-VPM light stimulation to the same pair of cells. SEM is shown as shaded color around the mean. V_m mark fosGFP$^+$ / fosGFP$^-$ (mV): –64.4 / –61.0.

(F-H) Analysis of 6 pairs of neurons revealed no significant differences in (F) latency, (G) amplitude, and (H) onset slope in fosGFP$^+$ neurons compared to fosGFP$^-$ neurons triggered by 3 ms light-evoked VPM stimulation. Gray filled circles correspond to example pair in (C)-(E). Red circles with error bars show mean ± SEM.

(I) Population average of the synaptic response to VPM light stimulation in neighboring fosGFP$^+$ and fosGFP$^-$ neurons (n = 6). Shaded background around the mean shows SEM. V_m mark fosGFP$^+$ / fosGFP$^-$ (mV): -65.5/ -65.6.

Figure 8. Optogenetic Stimulation of the Thalamic POm Nucleus Reveals Earlier and Larger Amplitude Synaptic Responses in fosGFP$^+$ Neurons.

(A) Schematic of two-photon targeted dual recording setup with optical fiber (cyan) inserted into the POm thalamic nucleus for ChR2 stimulation.
(B) Fluorescence image of a thalamocortical slice showing POm ChR2-GFP infection site in the thalamus and axonal projections in cortex; white schematic outlines of the brain structures are from the same slice under bright field illumination. Scale bar, 1 mm.
(C) Four single trial responses from the same pair of cells to 3 ms blue light stimulation (cyan bar) of POm. Examples correspond to anatomy in (B). V_m mark fosGFP$^+$ / fosGFP$^-$ (mV) from top to bottom: –54.7 / –60.4; –56.0 / –61.2; –56.5 / –64.0; –56.6 / –60.1.
(D) Trial-by-trial measurements of latency from the pair in (C) show an earlier responses in fosGFP$^+$ neurons compared to fosGFP$^-$ neurons (n = 28 trials).
(E) Averaged subthreshold response to ChR2-POm light stimulation for the same pair of cells. Shaded color around the mean shows SEM. V_m mark fosGFP$^+$ / fosGFP- (mV): –57.6 / –61.5.
(F-H) Analysis of eight pairs of neurons revealed a significantly (F) shorter latency, (G) larger amplitude, and (H) faster onset slope in fosGFP$^+$ neurons than fosGFP$^-$ neurons triggered by 3 ms light-evoked POm stimulation. Gray filled circles correspond to example pair in (C)-(E). Red circles with error bars show mean ± SEM.
(I) Population average of the synaptic response to POm light stimulation in neighboring fosGFP$^+$ and fosGFP$^-$ neurons (n = 8). Shaded background around the mean shows SEM. V_m mark fosGFP$^+$ / fosGFP$^-$ (mV): -62.9/ -63.0.

Figure 1

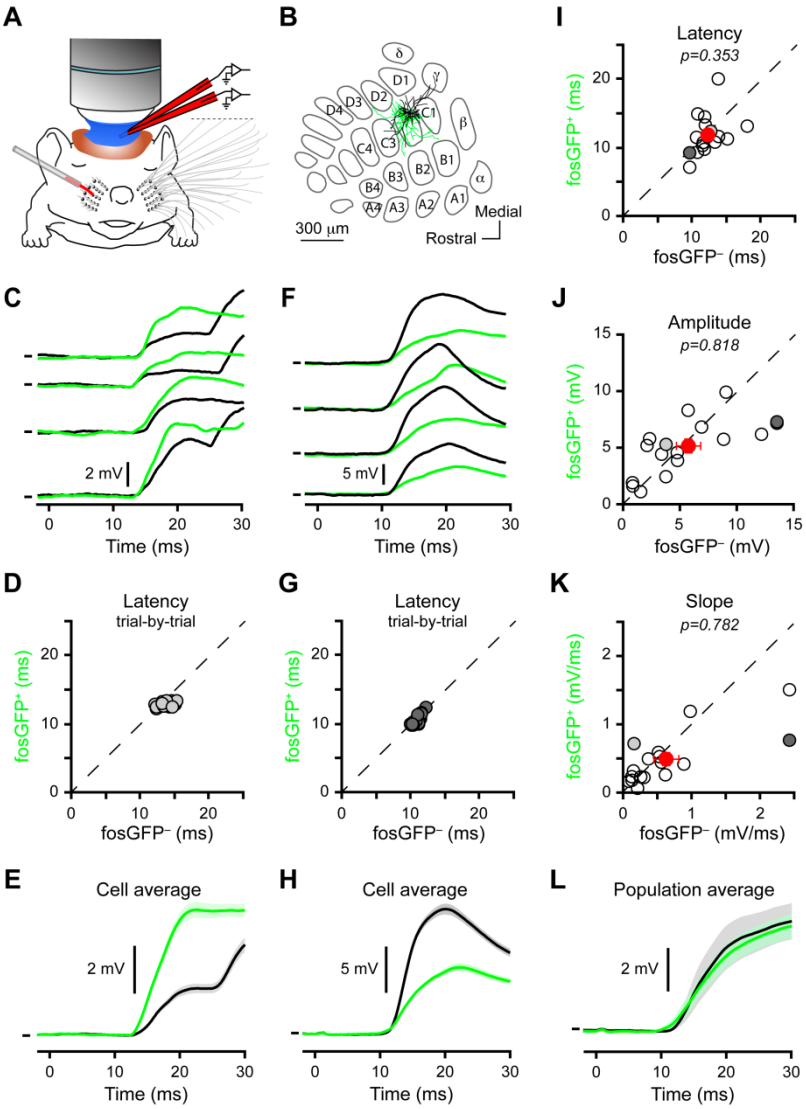
A
B
I
Latency
p=0.353
fosGFP⁺ (ms)
fosGFP⁻ (ms)
δ
γ
D1
D2
D3
D4
C1
C2
C3
C4
β
B1
B2
B3
B4
α
A1
A2
A3
A4
300 μm
Medial
Rostral
C
F
J
2 mV
5 mV
Time (ms)
Amplitude
p=0.818
fosGFP⁺ (mV)
fosGFP⁻ (mV)
D
G
K
Latency
trial-by-trial
Slope
p=0.782
fosGFP⁺ (mV/ms)
fosGFP⁻ (mV/ms)
E
H
L
Cell average
Population average

Figure 2

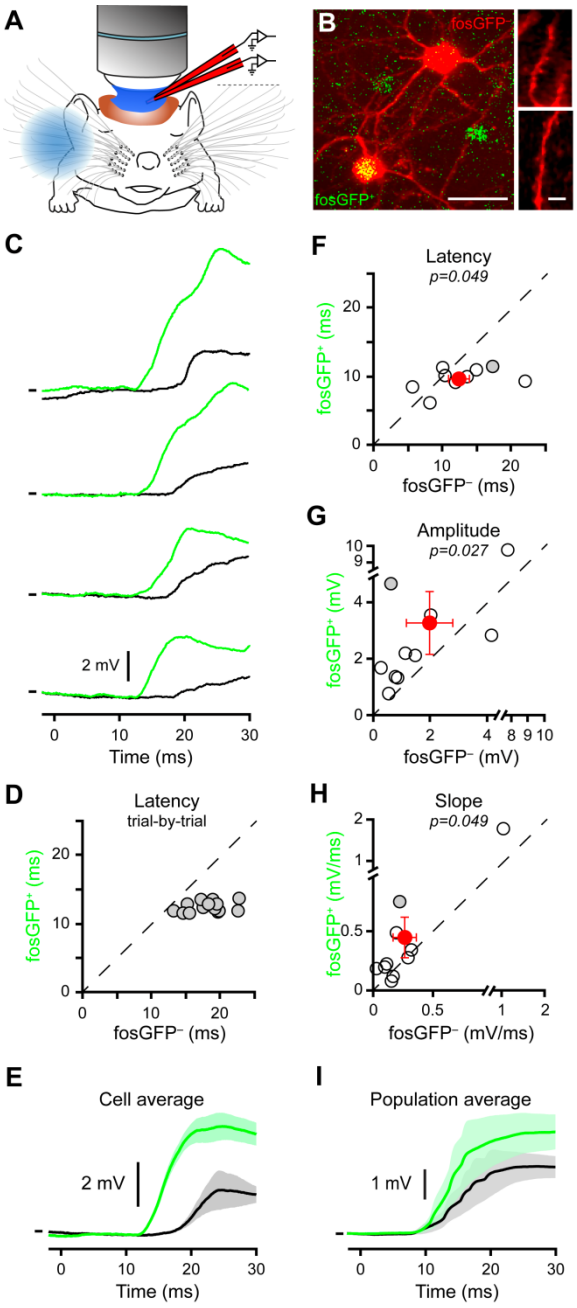
A
B
fosGFP⁻
fosGFP⁺
C
2 mV
0
10
20
30
Time (ms)
F
Latency
p=0.049
fosGFP⁺ (ms)
fosGFP⁻ (ms)
G
Amplitude
p=0.027
fosGFP⁺ (mV)
fosGFP⁻ (mV)
D
Latency
trial-by-trial
fosGFP⁺ (ms)
fosGFP⁻ (ms)
H
Slope
p=0.049
fosGFP⁺ (mV/ms)
fosGFP⁻ (mV/ms)
E
Cell average
2 mV
Time (ms)
I
Population average
1 mV
Time (ms)

Figure 3

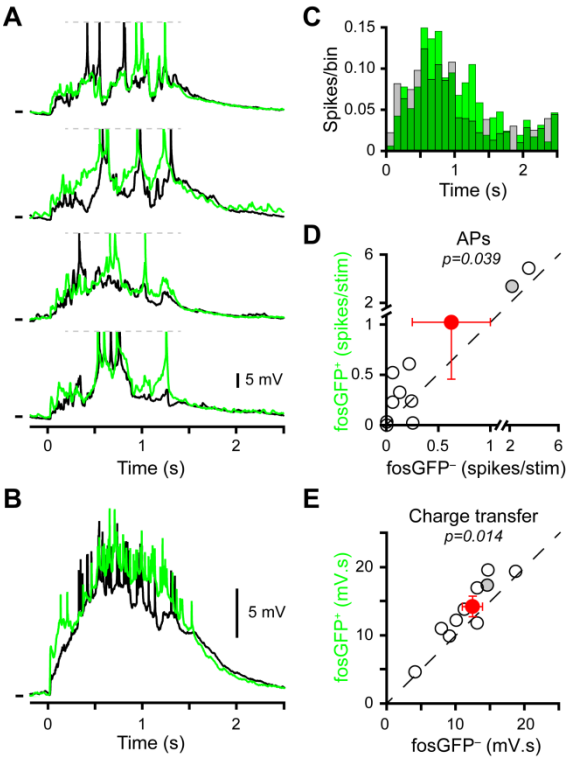
A
5 mV
Time (s)
B
5 mV
Time (s)
C
Spikes/bin
Time (s)
D
APs
p=0.039
fosGFP+ (spikes/stim)
fosGFP− (spikes/stim)
E
Charge transfer
p=0.014
fosGFP+ (mV.s)
fosGFP− (mV.s)

Figure 4

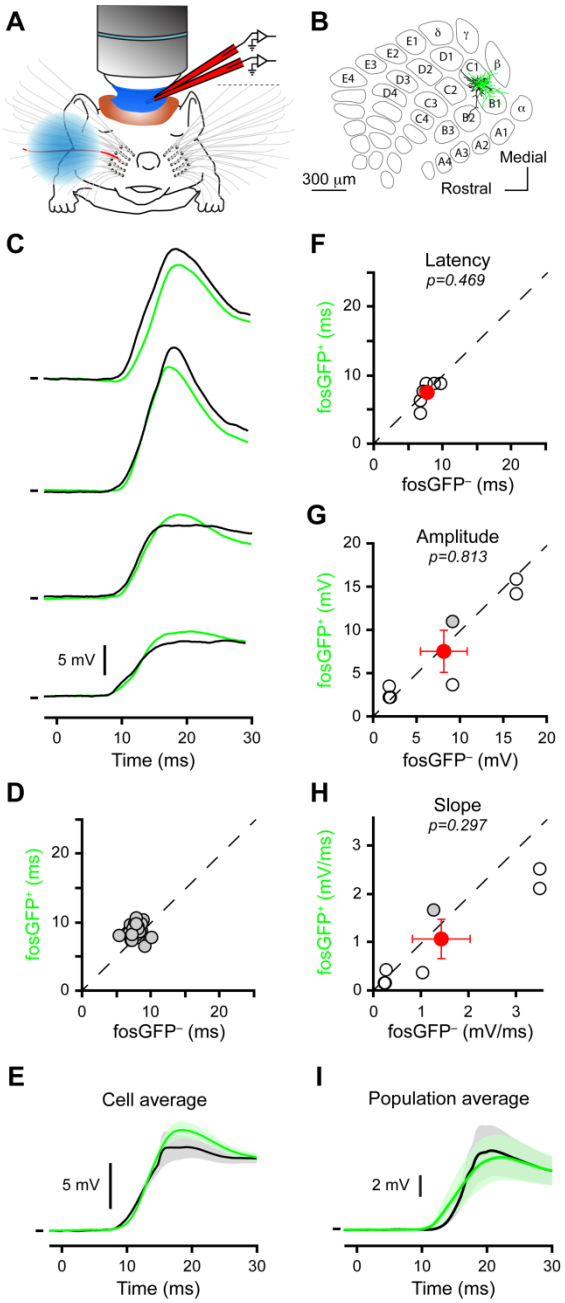
A
B
δ
γ
E1
E2
D1
E3
D2
C1
β
E4
D3
C2
B1
α
D4
C3
C4
B2
B3
A1
A2
A3
A4
300 µm
Medial
Rostral
C
5 mV
0
10
20
30
Time (ms)
F
Latency
p=0.469
fosGFP⁺ (ms)
fosGFP⁻ (ms)
G
Amplitude
p=0.813
fosGFP⁺ (mV)
fosGFP⁻ (mV)
D
fosGFP⁺ (ms)
fosGFP⁻ (ms)
H
Slope
p=0.297
fosGFP⁺ (mV/ms)
fosGFP⁻ (mV/ms)
E
Cell average
5 mV
Time (ms)
I
Population average
2 mV
Time (ms)

Figure 5

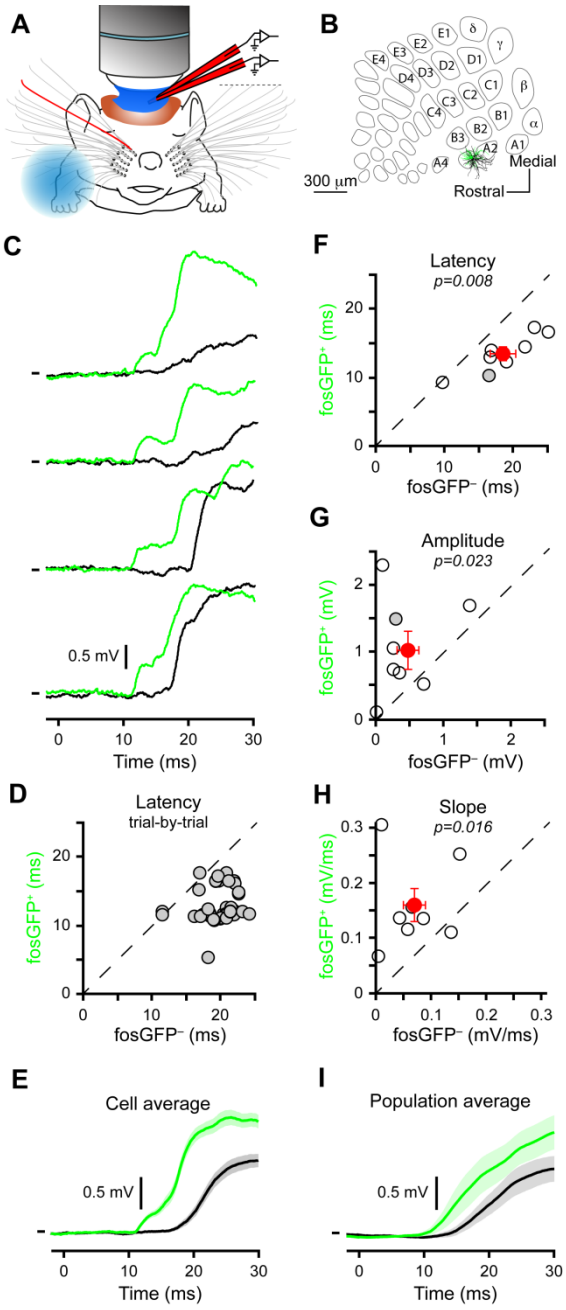
A
B
E1
δ
γ
E2
E3
E4
D1
D2
D3
D4
C1
β
C2
C3
C4
B1
α
B2
B3
A1
A2
A4
Medial
Rostral
300 μm
C
0.5 mV
0
10
20
30
Time (ms)
F
Latency
p=0.008
fosGFP⁺ (ms)
fosGFP⁻ (ms)
G
Amplitude
p=0.023
fosGFP⁺ (mV)
fosGFP⁻ (mV)
D
Latency
trial-by-trial
fosGFP⁺ (ms)
fosGFP⁻ (ms)
H
Slope
p=0.016
fosGFP⁺ (mV/ms)
fosGFP⁻ (mV/ms)
E
Cell average
0.5 mV
Time (ms)
I
Population average
0.5 mV
Time (ms)

Figure 6

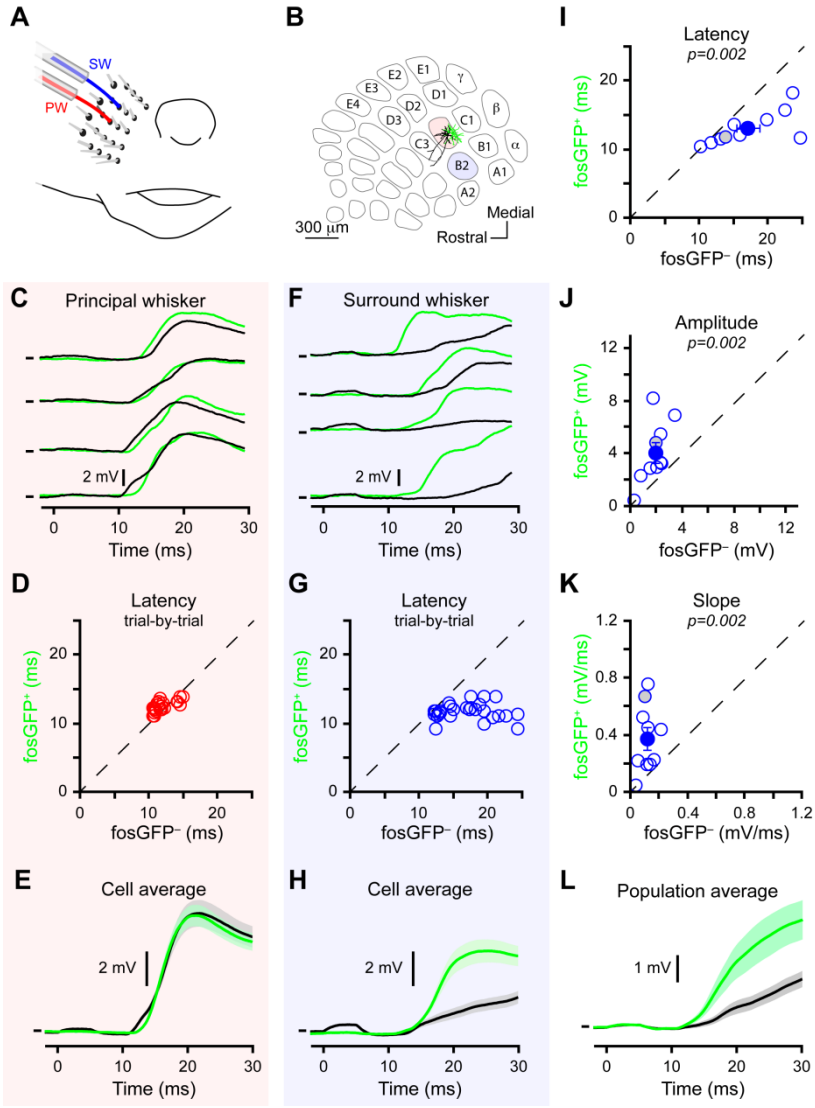
A
SW
PW
B
E1
E2
E3
E4
D1
D2
D3
C1
C3
B1
B2
A1
A2
α
β
γ
300 µm
Medial
Rostral
I
Latency
p=0.002
fosGFP⁺ (ms)
fosGFP⁻ (ms)
C
Principal whisker
2 mV
Time (ms)
F
Surround whisker
2 mV
Time (ms)
J
Amplitude
p=0.002
fosGFP⁺ (mV)
fosGFP⁻ (mV)
D
Latency
trial-by-trial
fosGFP⁺ (ms)
fosGFP⁻ (ms)
G
Latency
trial-by-trial
fosGFP⁺ (ms)
fosGFP⁻ (ms)
K
Slope
p=0.002
fosGFP⁺ (mV/ms)
fosGFP⁻ (mV/ms)
E
Cell average
2 mV
Time (ms)
H
Cell average
2 mV
Time (ms)
L
Population average
1 mV
Time (ms)

Figure 7

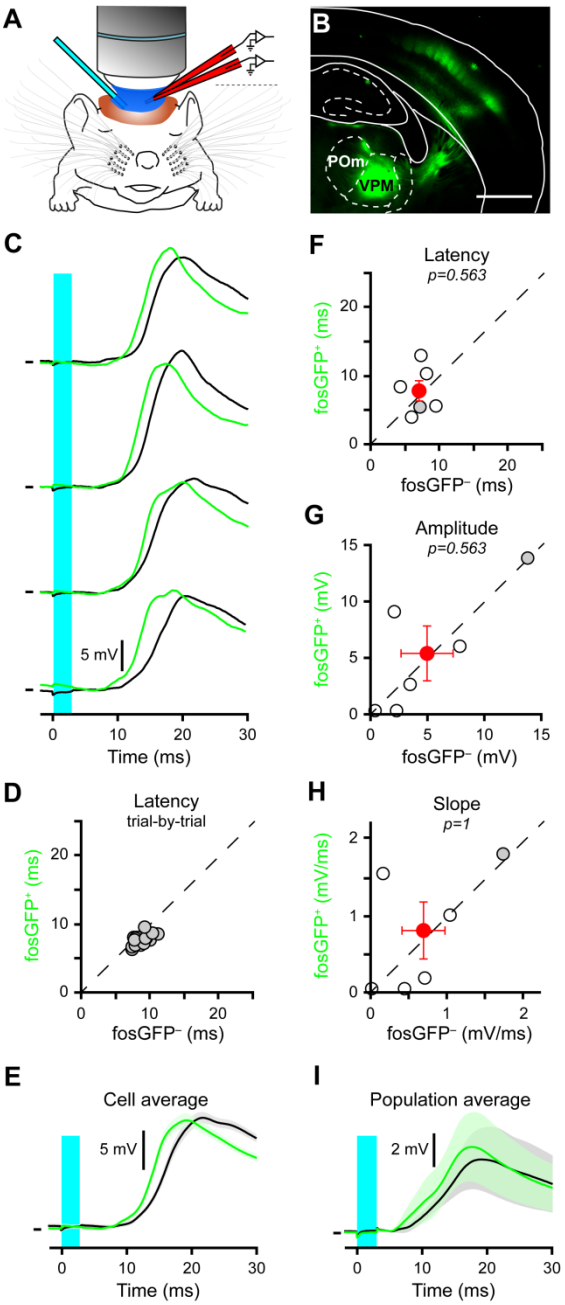
A
B
POm
VPM
C
5 mV
Time (ms)
F
Latency
p=0.563
fosGFP⁺ (ms)
fosGFP⁻ (ms)
G
Amplitude
p=0.563
fosGFP⁺ (mV)
fosGFP⁻ (mV)
D
Latency
trial-by-trial
fosGFP⁺ (ms)
fosGFP⁻ (ms)
H
Slope
p=1
fosGFP⁺ (mV/ms)
fosGFP⁻ (mV/ms)
E
Cell average
5 mV
Time (ms)
I
Population average
2 mV
Time (ms)

Figure 8

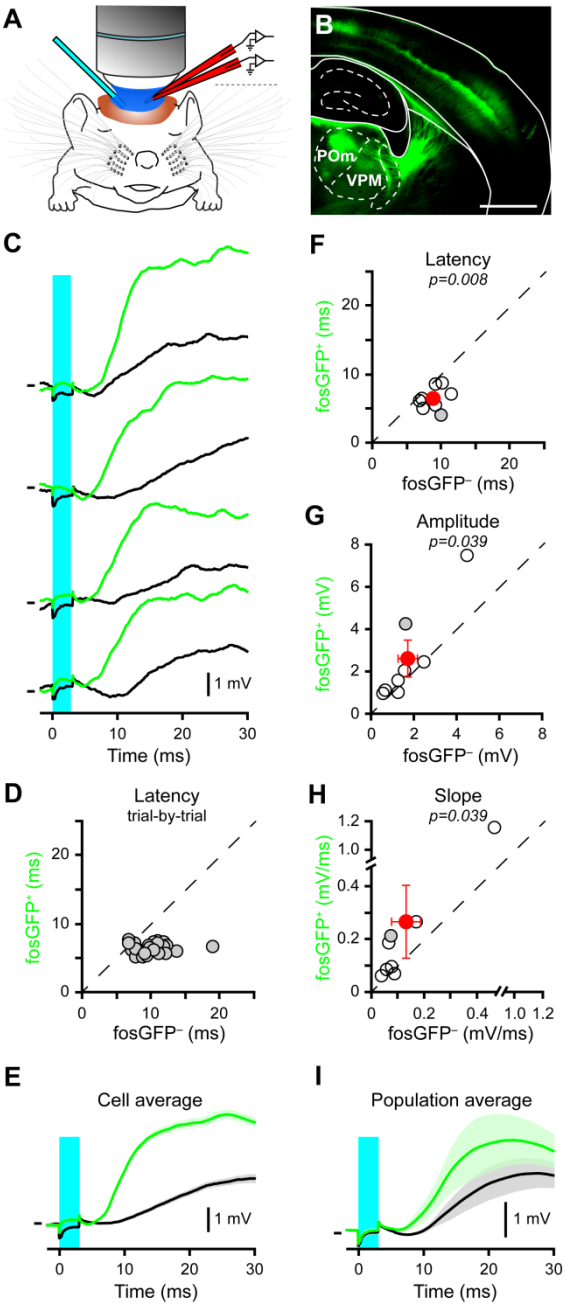
A
B
POm
VPM
C
1 mV
0
10
20
30
Time (ms)
F
Latency
p=0.008
fosGFP⁺ (ms)
fosGFP⁻ (ms)
G
Amplitude
p=0.039
fosGFP⁺ (mV)
fosGFP⁻ (mV)
D
Latency
trial-by-trial
fosGFP⁺ (ms)
fosGFP⁻ (ms)
H
Slope
p=0.039
fosGFP⁺ (mV/ms)
fosGFP⁻ (mV/ms)
E
Cell average
1 mV
Time (ms)
I
Population average
1 mV
Time (ms)

SUPPLEMENTAL INFORMATION

Cortical fosGFP expression reveals broad receptive field excitatory neurons targeted by POm

Jean-Sébastien Jouhanneau, Leiron Ferrarese, Luc Estebanez, Nick J. Audette, Michael Brecht, Alison L. Barth and James F.A. Poulet

Supplemental Figures

Figure S1, related to Figures 1-8. In vivo characterization of GFP fluorescence in the fosGFP mouse.

(A) In vivo 2-photon fluorescence image taken before dual patch recordings from neighboring fosGFP$^+$ and fosGFP$^-$ neurons. The fosGFP$^+$ and fosGFP$^-$ cells recorded in this experiment are marked with white arrows. (B) Green fluorescence distribution after background subtraction from the example experiment in (A) (n = 42 cells in this example field of view). (C) The same data but with the green fluorescence distribution normalized to the brightest cell of the field from the example experiment in (A). In (B) and (C) the recorded fosGFP$^+$ and fosGFP$^-$ neurons from (A) are colored in green and black respectively and marked by an arrow. Dashed line shows the threshold for selecting fosGFP$^+$ and fosGFP$^-$ neurons. (D) Population distribution of green fluorescence signal in 449 cells from 10 mice. (E) Fluorescence of recorded fosGFP$^+$ (green) and fosGFP$^-$ (black) neurons recorded in 10 dual recording show a significant difference in fosGFP fluorescence signal. Filled circles are mean signal ± s.e.m.. (F) Population distribution of green fluorescence signal normalized to the brightest neuron in the corresponding field of view, n = 449 cells, 10 mice. (G) FosGFP fluorescence of recorded pairs normalized to the brightest cell of the corresponding field of view. Dashed line shows the threshold for selecting fosGFP$^+$ or fosGFP$^-$ neurons. Filled circles are mean signal ± s.e.m.. (H) Percentage of fosGFP$^+$ neurons seen across 10 mice using normalized fluorescence.

Figure S2, related to Figure 3. FosGFP$^+$ neurons fire more action potentials than fosGFP$^-$ neurons during spontaneous activity under urethane anesthesia.

(A) In vivo red and green fluorescence image taken during targeting of neighboring fosGFP$^+$ and fosGFP$^-$ neurons. Alexa 594 (red fluorescence) from the patch pipettes fills the extracellular space creating shadows of the cell soma. White dashed lines indicate position of recording pipettes directed toward a pair of fosGFP$^+$ and fosGFP$^-$ neurons targeted for recording. Scale bar, 20 µm. (B) Left, in vivo merged Z-stack image of same cell pair after patch clamp recordings. Scale bar, 20 µm. Right, short section of dendrite from a fosGFP$^+$ (top) and a fosGFP$^-$ (below) neuron showing spines. Scale bar, 5 µm. (C) Biocytin stain of same pair of cells. Scale bar, 20 µm. (D) Example recording section of spontaneous activity from the same pair of neurons. (E) Upstate-triggered average of same pair of neurons (n = 30 Upstates). V_m mark fosGFP$^+$/fosGFP$^-$ (mV): –57.1/–58.5. (F) Zoom in from the dashed box in (E) showing the onset of the averaged Upstate. (G) Firing rate is significantly higher in fosGFP$^+$ neurons during spontaneous activity. (H) V_m charge transfer (integral) during the Upstate is larger in fosGFP$^+$ than fosGFP$^-$ neurons. (I) Onset slope of Upstate is significantly steeper in fosGFP$^+$ than fosGFP$^-$ neurons. Grey filled circles indicate the example recording in (A-F). Circles with error bars show mean ± s.e.m. (n = 7).

Figure S3, related to Figures 1-8. Quantification of dendritic branching of fosGFP$^+$ and fosGFP$^-$ neurons stained with biocytin during dual whole-cell recordings.

(A) 6 reconstructed pairs of fosGFP$^+$ (green) and fosGFP$^-$ (black) neurons. (B) Quantification of the numbers of dendritic branches, dendritic branchpoints, dendritic ends, total dendritic length, dendritic perimeter and area of dendritic arborization showed no significant differences from the 6 reconstructed pairs in (A). (C) FosGFP$^+$ neurons have a larger soma than fosGFP$^-$ neurons (n = 18 pairs, 10 in vivo measurements from images taken before patch clamp recordings, 8 measurements from post-hoc biocytin-filled pairs). (D) Overlay of the position of cell somata from 6 pairs of fosGFP$^+$ / fosGFP$^-$ neurons on their corresponding layer 4 barrel. (E) Graph showing no significant difference in the distance from the border of the barrel comparing fosGFP$^-$ and fosGFP$^+$ neurons.

Figure S4, related to Figures 1-8. FosGFP$^+$ neurons project with equal likelihood to motor cortex, secondary somatosensory cortex and contralateral primary somatosensory cortex.

(A) Schematic showing CTB-Alexa 594 injection site in whisker motor cortex (M1). (B) Fluorescence imaging of coronal slice showing the location of CTB-Alexa 594 injection site in M1. (C) Example (top) CTB$^+$ / fosGFP$^-$ and (bottom) CTB$^+$ / fosGFP$^+$ neurons in barrel cortex. (D) Probability of a CTB$^+$ neuron projecting to M1 also being fosGFP$^+$. (E) Schematic showing CTB-Alexa 594 injected to S2. (F) Fluorescence imaging showing the location of CTB-Alexa 594 injection in S2. (G) Example (top) CTB$^+$ / fosGFP$^-$ and (bottom) CTB$^+$ / fosGFP$^+$ neurons projecting to secondary somatosensory cortex (S2). (H) Probability of a CTB$^+$ neuron projecting to S2 also being fosGFP$^+$. (I) Schematic showing CTB-Alexa 594 injected to contralateral S1 (cS1). (J) Fluorescence imaging showing the location of CTB-Alexa 594 injection in cS1. (K) Example (top) CTB$^+$ / fosGFP$^-$ and (bottom) CTB$^+$ / fosGFP$^+$ neurons projecting to cS1. (L) Probability of a CTB$^+$ neuron projecting to cS1 also being fosGFP$^+$.

Figure S5, related to Figure 8. POm neurons show short latency responses to airpuff stimulation of the whiskers.

(A) Example bright field image of coronal brain slice. Blue: DiO fluorescent mark left by extracellular electrode. (B) Close up of the thalamus from the same slice, note end of electrode track located in POm. (C) Example short-latency neuron. Whisker movement starts at t = 0. Left top: Spike shapes on the eight close by recording sites of the electrode. Left bottom: autocorrelogram of spike train. Right: PSTH of spike train triggered by airpuff on whisker pad. (D) Same as (C) for a long-latency neuron. (E) Left: Average PSTH of all units (see methods, n = 91 cells from 3 mice). Right: zoom of the same PSTH around stimulus onset. Green dashed line represents the mean synaptic response latency of the fosGFP$^+$ cells to airpuff stimulus. (F) Left: Latency histogram of neurons with significant responses (66 units). Median latency was 19.5 ms, and mean latency was 82.7 ± 14.8 ms. Right: zoom of the same histogram around stimulus onset. Green dashed line represents the mean synaptic response latency of the fosGFP$^+$ cells to airpuff stimulus.

Figure S6, related to Figures 7 and 8. Localization of POm and VPM ChR2-GFP viral infection sites.

(A) Schematic showing location of all POm infections shown in Figure 8 as dots, red dot is example shown in B. Outline taken from bright field imaging. Scale bar, 1 mm. (B) Zoomed overlay of the fluorescent image showing the POm targeted ChR2-GFP expression site 2 weeks after infection and the bright field image. Borders between VPM and POm are shown as white dashed lines. Scale bar, 200 μm. (C) POm axonal projections in a coronal slice of the barrel cortex from experiment shown in B. Pial surface shown as white dashed line. Scale bar, 100 μm. (D) Schematic showing locations of ChR2-GFP infections in VPM shown in Figure 7, red dot indicates example in E. Outline taken from bright field imaging. Scale bar, 1 mm. (E) Example ChR2-GFP infection site 2 weeks after injection. Scale bar, 200 μm. (F) VPM axonal projection patterns in barrel cortex for experiment shown in (E). Scale bar, 100 μm.

Supplemental Experimental Procedures

Retrograde axonal staining

Cholera toxin B 594 (CTxB; 0.33% in phosphate buffer pH 7.15, 400nL; Life Technologies) was injected into primary motor cortex (M1) at 1 mm rostral / 1 mm lateral to bregma; or at 0.6 mm caudal / 4.1 mm lateral to bregma for S2 in fosGFP transgenic mice aged P17-22. Animals were allowed to recover for 4-7 days to enable retrograde transport of CTxB. Cells in L2 of S1 were imaged for CTxB cytoplasmic label and nuclear fosGFP in live tissue (acute brain slices, 350 µm thick, ACSF). In a subset of samples, animals were perfused with PFA, brains were cryo-protected in sucrose, and sectioned to 50µm slices before imaging in an anti-fade solution. Overlap results were similar between live and fixed samples; numbers were combined and analyzed together. For each animal the injection site was confirmed by post-hoc fluorescent imaging with reference to the Paxinos mouse brain atlas.

Extracellular recordings from POm

A 1 mm diameter craniotomy was performed at coordinates –1.8 mm posterior, 1.25 mm lateral to Bregma in urethane anesthetized fosGFP, P18-22 mice (n = 3). A Neuronexus Buszaki32 silicon probes (8 site polytrode, 4 shanks) coated with DiO dye (Life Technologies, D-3898) was then slowly (~ 2 µm / sec) lowered vertically into POm (depth 2700-3300 µm). Electrophysiological data were continuously recorded at 22 kHz from the 32 channels of the silicon probes by a Digital Lynx 4SX (Neuralynx). During the recording, airpuffs (10 ms, 20 p.s.i.) were applied on the right whisker pad every 4 s.

Spike extraction, automatic clustering and final manual cluster selection and merging were performed using the KlustaSuite (http://klusta-team.github.io/). After the automatic spike sorting procedure, units with noisy spike shapes were discarded, and we iteratively applied the following steps: units with very high-frequency bursts (< 2 ms in autocorrelogram) or noisy spike shapes were discarded and units with similar shapes and autocorrelograms were merged. For PSTH computation and further analysis, we retained only neurons that fired more than 50 spikes and displayed an

average firing rate of more than 0.5 Hz across the recording. Detection of significant responses was performed on PSTHs with a 5 ms binning. For each neuron, the baseline was computed on the 100 ms before airpuff onset. Significance of sensory responses and their latencies were detected by using a Poisson exact test ($P < 0.01$, Poisson.exact command in R) to compare the baseline with the activity on each of the 5 ms bins of the PSTH. Latencies were computed with respect to the time of the first movement of the whisker generated by the airpuff, as measured with a high-speed camera at 600 Hz.

Supp Figure 1

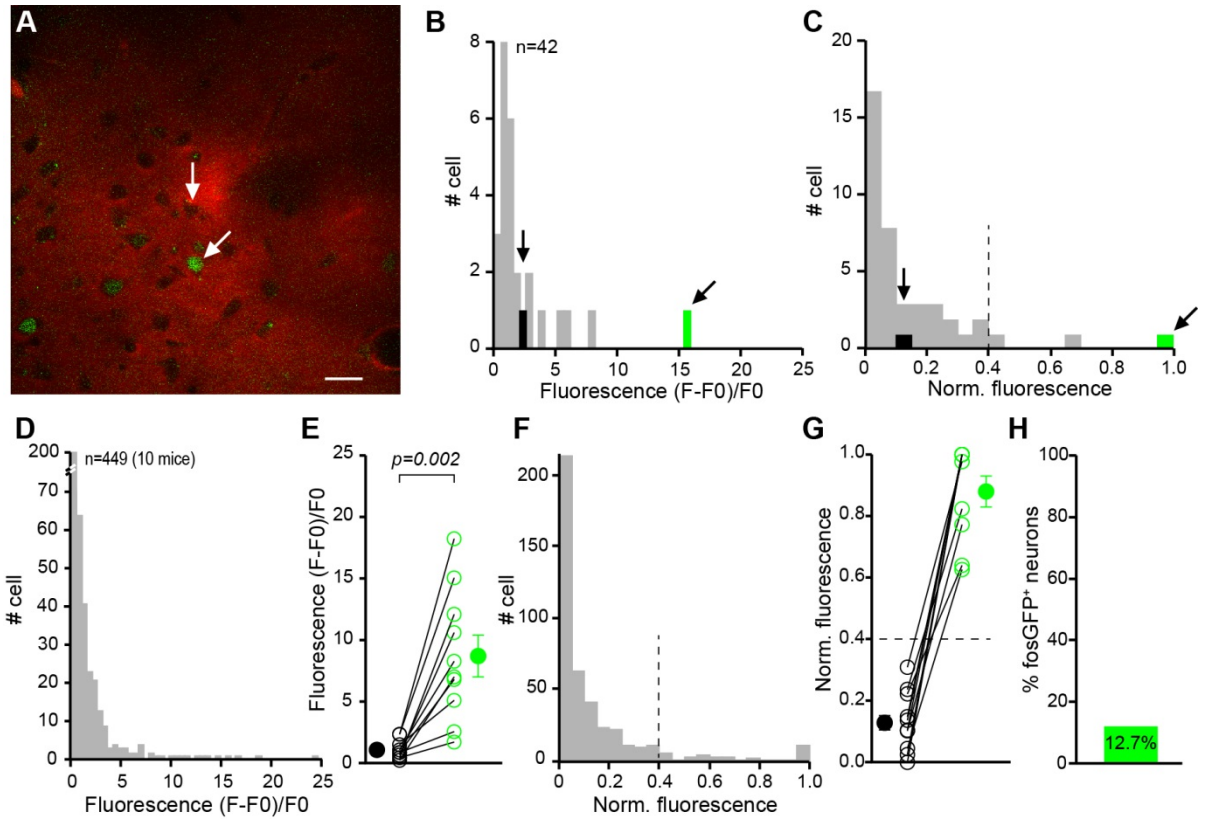

Supp Figure 2

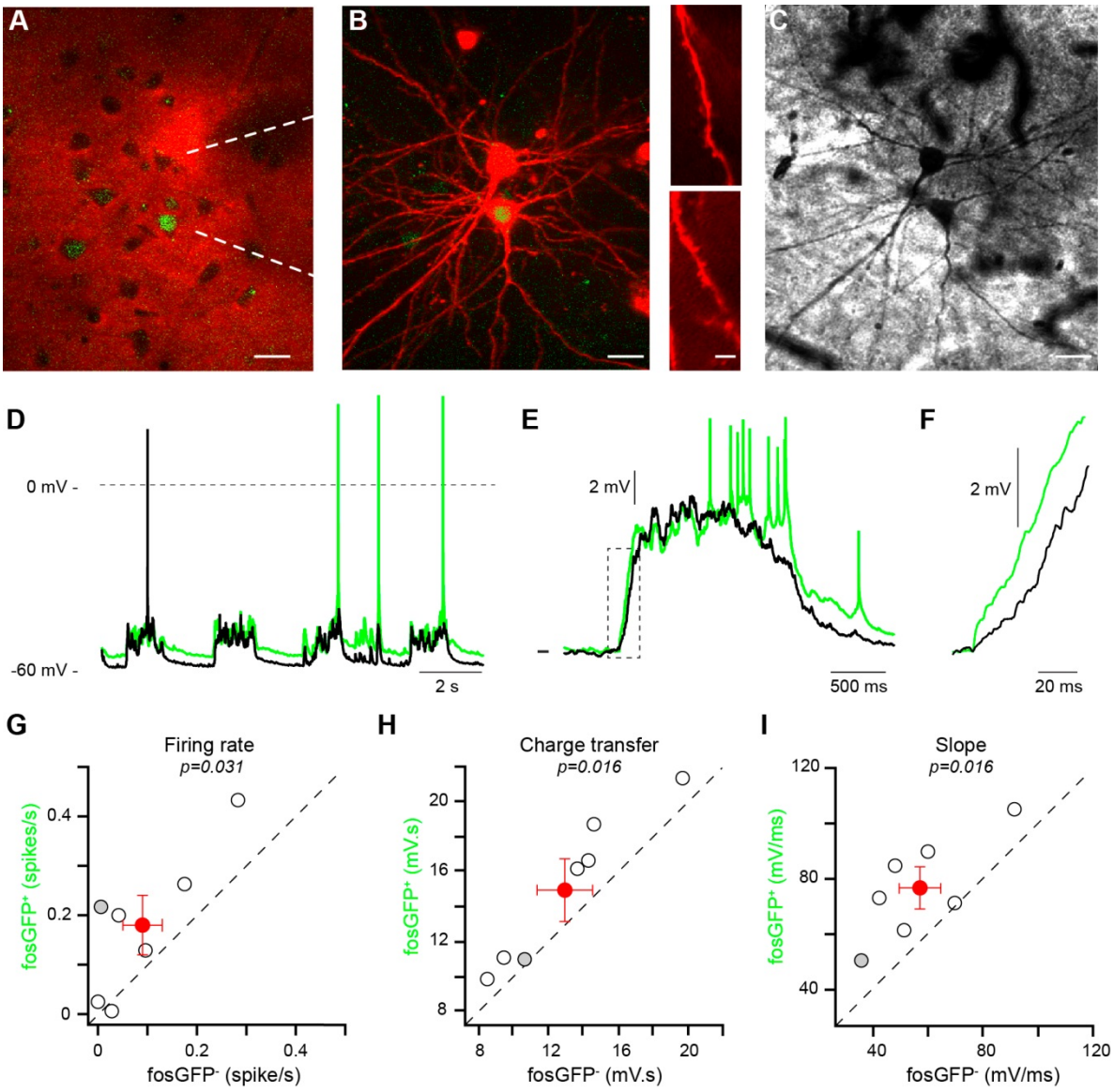

Supp Figure 3

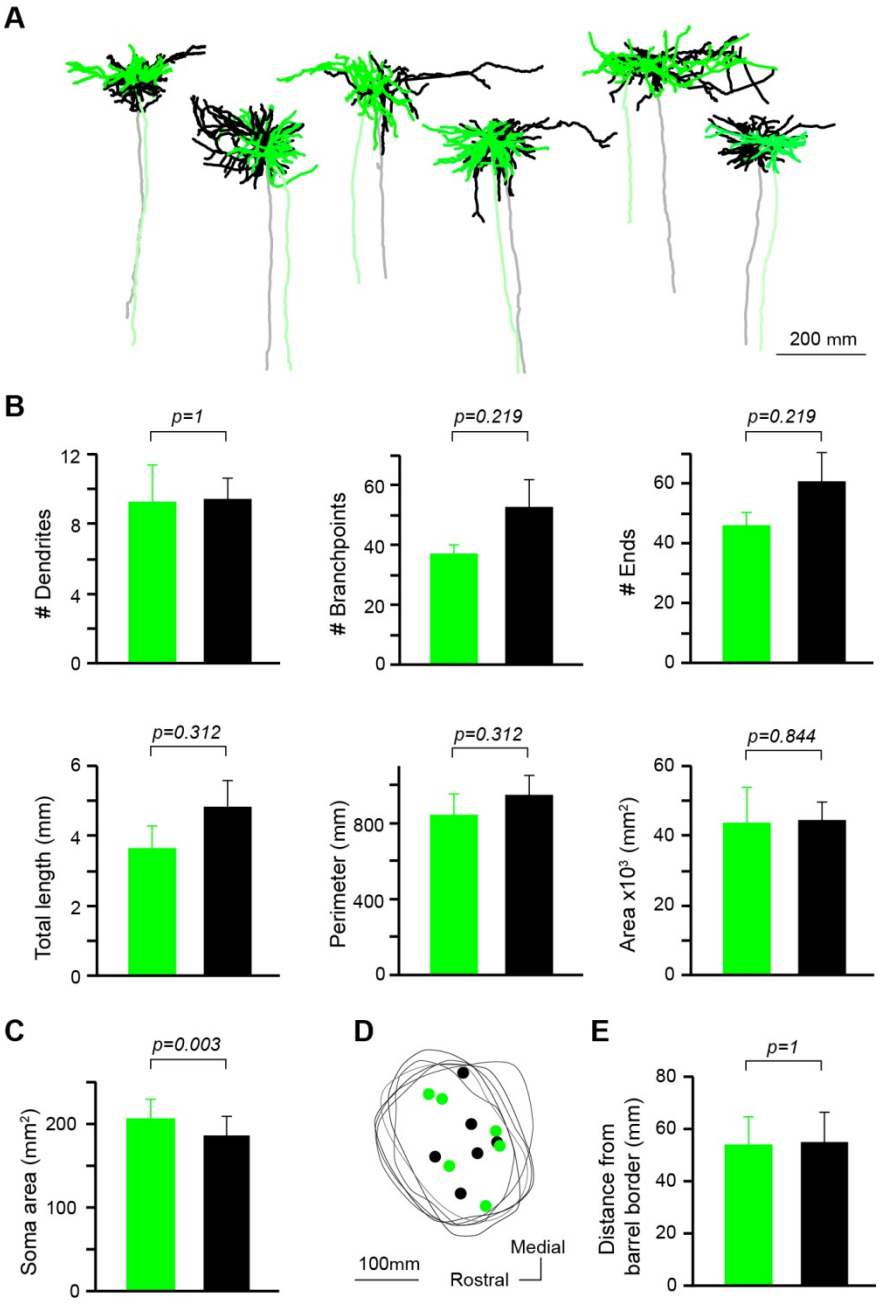

Supp Figure 4

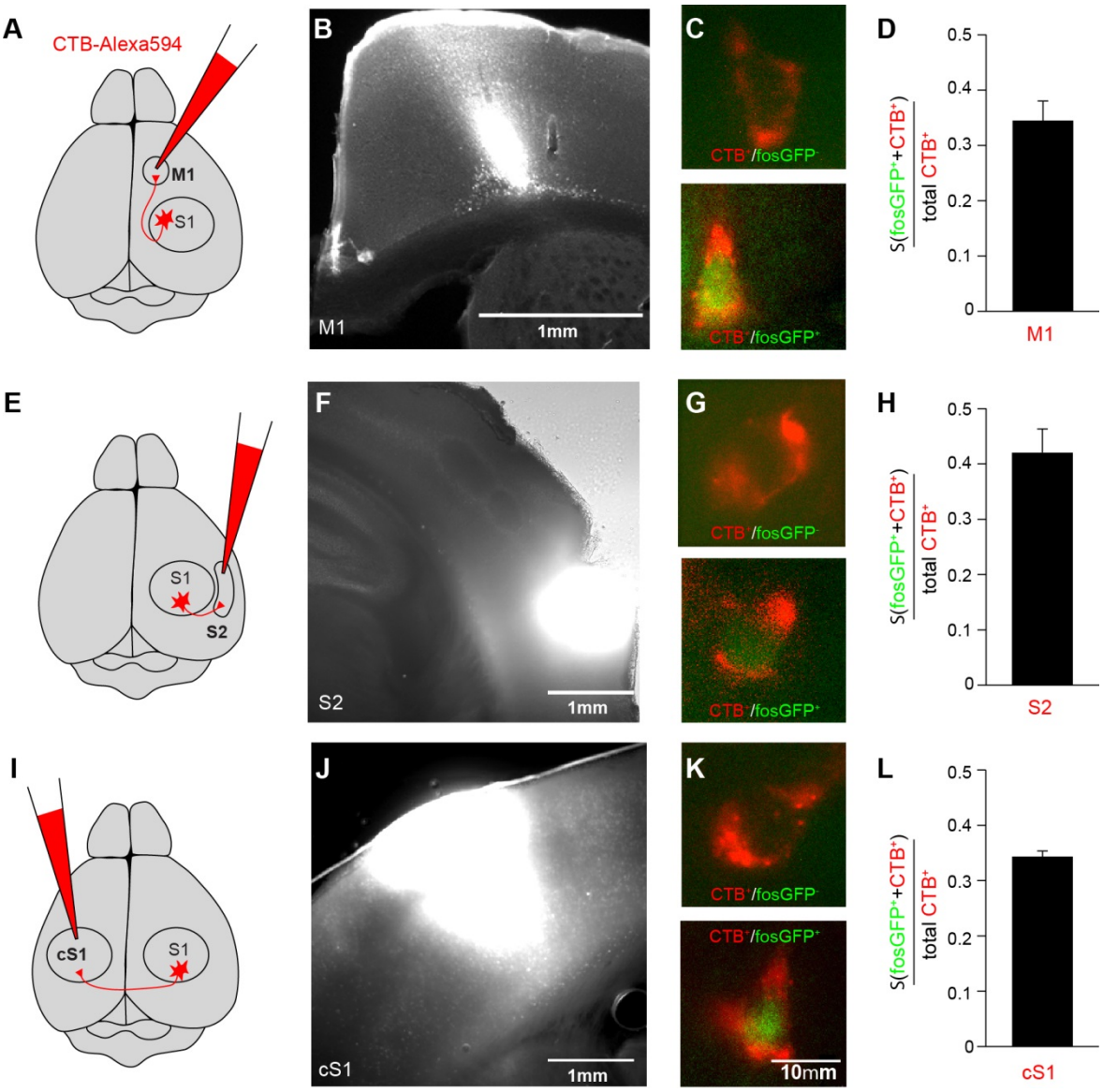

Supp Figure 5

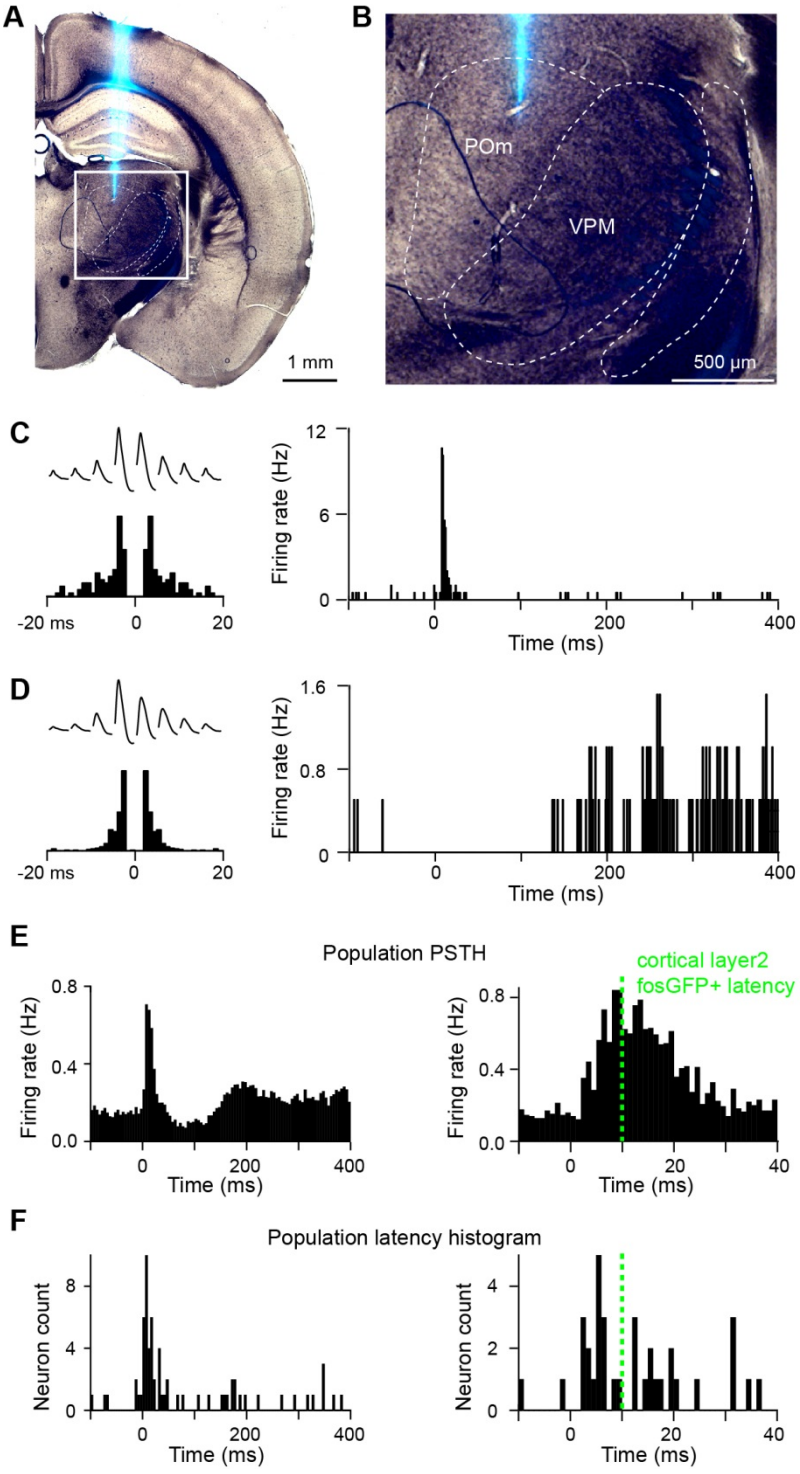

Supp Figure 6